

This is an Open Access document downloaded from ORCA, Cardiff University's institutional repository: <https://orca.cardiff.ac.uk/id/eprint/109170/>

This is the author's version of a work that was submitted to / accepted for publication.

Citation for final published version:

Khaki, M., Forootan, Ehsan , Kuhn, M., Awange, J., van Dijk, A.I.J.M., Schumacher, M. and Sharifi, M.A. 2018. Determining water storage depletion within Iran by assimilating GRACE data into the W3RA hydrological model. *Advances in Water Resources* 114 , pp. 1-18. 10.1016/j.advwatres.2018.02.008

Publishers page: <http://dx.doi.org/10.1016/j.advwatres.2018.02.008>

Please note:

Changes made as a result of publishing processes such as copy-editing, formatting and page numbers may not be reflected in this version. For the definitive version of this publication, please refer to the published source. You are advised to consult the publisher's version if you wish to cite this paper.

This version is being made available in accordance with publisher policies. See <http://orca.cf.ac.uk/policies.html> for usage policies. Copyright and moral rights for publications made available in ORCA are retained by the copyright holders.



Determining Water Storage Depletion within Iran by Assimilating GRACE data into the W3RA Hydrological Model

M. Khaki^{a,1}, E. Forootan^b, M. Kuhn^a, J. Awange^a, A. I. J. M. van Dijk^c, M. Schumacher^d, M. A. Sharifi^{e,f}

^a*School of Earth and Planetary Sciences, Discipline of Spatial Sciences, Curtin University, Perth, Australia.*

^b*School of Earth and Ocean Sciences, Cardiff University, Cardiff, UK.*

^c*Fenner School of Environment and Society, the Australian National University, Canberra, Australia.*

^d*School of Geographical Sciences, University of Bristol, Bristol, UK.*

^e*Faculty of Surveying and Geospatial Engineering, College of Engineering, University of Tehran, Iran.*

^f*Research Institute of Geoinformation Technology (RIGT), College of Engineering, University of Tehran, Iran.*

Abstract

Groundwater depletion, due to both unsustainable water use and a decrease in precipitation, has been reported in many parts of Iran. In order to analyze these changes during the recent decade, in this study, we assimilate Terrestrial Water Storage (TWS) data from the Gravity Recovery And Climate Experiment (GRACE) into the World-Wide Water Resources Assessment (W3RA) model. This assimilation improves model derived water storage simulations by introducing missing trends and correcting the amplitude and phase of seasonal water storage variations. The Ensemble Square-Root Filter (EnSRF) technique is applied, which showed stable performance in propagating errors during the assimilation period (2002-2012). Our focus is on sub-surface water storage changes including groundwater and soil moisture variations within six major drainage divisions covering the whole Iran including its eastern part (East), Caspian Sea, Centre, Sarakhs, Persian Gulf and Oman Sea, and Lake Urmia. Results indicate an average of -8.9 mm/year groundwater reduction within Iran during the period 2002 to 2012. A similar decrease is also observed in soil moisture storage especially after 2005. We further apply the canonical correlation analysis (CCA) technique to relate sub-surface water storage changes to climate (e.g., precipitation) and anthropogenic (e.g., farming) impacts. Results indicate an average correlation of 0.81 between rainfall and groundwater variations and also a large impact of anthropogenic activities (mainly for irrigations) on Iran's water storage depletions.

Keywords: Iran, Groundwater Storage, Data Assimilation, Canonical Correlation Analysis, GRACE, W3RA Hydrological Model, Water Storage Depletion

Email address: Mehdi.Khaki@postgrad.curtin.edu.au (M. Khaki)

¹Contact details: Department of Spatial Sciences, Curtin University, Perth, Australia, Email: Mehdi.Khaki@postgrad.curtin.edu.au, Tel: 0061410620379

57
58
59 **1. Introduction**
60

61
62 Water scarcity has become a serious issue in the Islamic Republic of Iran (abbreviated
63 here as Iran) in recent years (e.g., Amery and Wolf, 2000; Wolf and Newton, 2007; Trigo
64 et al., 2010; Madani, 2014; Michel, 2017). With the increased extraction of groundwater, its
65 level has been reported to fall significantly (see, e.g., Sarraf et al., 2005; Motagh et al., 2008;
66 Mohammadi-Ghaleni and Ebrahimi, 2011; Van Camp et al., 2012; Afshar et al., 2016). There
67 have been studies that investigate surface and groundwater changes in Iran during the last
68 decade (2003 onward) mainly using Terrestrial Water Storage (TWS) data from the Gravity
69 Recovery And Climate Experiment (GRACE, Tapley et al., 2004). For example, Voss et al.
70 (2013) reported $\sim 143.6 \text{ km}^3$ reduction of freshwater from 2003 to 2009 over the north-central
71 area of the Middle East, which largely covers the Tigris-Euphrates Basin. Forootan et al.
72 (2014a) applied a statistical inversion to separate GRACE TWS using hydrological model out-
73 puts and altimetry data as a priori information, and found a decrease in water storage with
74 an average linear rate of $\sim -15 \text{ mm/year}$ between 2002 and 2011. A large negative trend (2003-
75 2012) in TWS was observed by Joodaki et al. (2014) using GRACE TWS data over the western
76 Iran and eastern Iraq.

77
78 Estimating sub-surface water storages is very important since they support the life in semi-
79 arid areas like Iran. Fatolazadeh et al. (2016) used the wavelet approach to improve estimates of
80 groundwater storage variations from GRACE and found a remarkable decrease in groundwater
81 in 2008, 2010 and particularly in 2011. Forootan et al. (2017) compared changes in water
82 storage and hydrological water fluxes in Iran using GRACE and climate reanalysis data. Their
83 results indicated that the decline of TWS in the Urmia and Tigris-Euphrates basins are greater
84 than the decrease in the monthly accumulated total water fluxes. Therefore, it was concluded
85 that the anthropogenic contribution on surface and groundwater flow is significant, and results
86 in the storage decline within Iran.

87
88 These studies have proved the effectiveness of GRACE to enhance the understanding of
89 water storage changes within the country. However, they do not provide a full understanding of
90 spatially distributed water resources changes in different water compartments in Iran. GRACE
91 TWS measures the summation of all water masses in the surface and sub-surface compart-
92 ment of the terrestrial water storage (vegetation, snow, surface waters, soil, groundwater, etc.).
93 Therefore, GRACE TWS must be separated into different storage compartments, which has
94 been achieved to date through a forward modeling or an inversion framework as is described in
95
96
97
98
99
100
101
102
103
104
105
106
107
108
109
110
111
112

113 Forootan et al. (2014a) and the literature mentioned before.

114
115 To complement previous attempts, the aims of this study are to (i) update hydrological
116
117 model simulations of sub-surface water storage changes (including water stored in the soil
118
119 and groundwater storage) within Iran using GRACE data assimilation, and (ii) investigate
120
121 climate and anthropogenic impacts on the estimated sub-surface water storages in (i). This
122
123 study is the first data assimilation attempt to integrate GRACE TWS into the World-Wide
124
125 Water Resources Assessment (W3RA; van Dijk, 2010) hydrological model over Iran. This
126
127 methodology has been implemented in studies to constrain the mass balance of hydrological
128
129 models over different river basins (e.g., Zaitchik et al., 2008; van Dijk et al., 2014; Eicker et al.,
130
131 2014; Reager et al., 2015; Giroto et al., 2016; Schumacher et al., 2016). The main rationale in
132
133 following this approach is that one relies on the physical processes, implemented in the model
134
135 equations, to separate GRACE TWS into water compartments (see similar arguments, e.g., in
136
137 Bertino et al., 2003). Thus, by generating ensemble members for a model derived water storage
138
139 simulation, we will compute a priori estimates of mass redistribution in the country. Then,
140
141 by assimilating GRACE data, while considering their uncertainty, we update (correct) these
142
143 model estimations. A similar concept has also been followed in studies in hydrology, climate,
144
145 and oceanography (see, e.g., Garner et al., 1999; Bennett, 2002; Kalnay, 2003; Schunk et al.,
146
147 2004; Lahoz et al., 2007; Khaki et al., 2017a,b). In addition, by applying data assimilation, we
148
149 will likely be able to reliably separate GRACE TWS data into different water compartments
150
151 since both model and observation errors are considered. Considering that the spatial resolution
152
153 of models is usually better than GRACE data, through the assimilation procedure, GRACE
154
155 observations are downscaled, and therefore, higher resolution estimations of water storages will
156
157 be available within the country (see also Schumacher et al., 2016; Khaki et al., 2018a).

158
159 Once improved model simulations are obtained, by assimilating GRACE TWS, relation-
160
161 ships between the model-derived groundwater and soil moisture storages and climatic variables
162
163 within Iran are investigated. To investigate the impacts of climate on the regional water stor-
164
165 age estimates, precipitation from satellite remote sensing, temperature, and vegetation changes
166
167 through the Normalized Difference Vegetation Index (NDVI) are used. Furthermore, anthro-
168
pogenic effects are explored using the changes in water use for farming, industry, and human
consumption. To this end, Canonical Correlation Analysis (CCA) is applied to provide an
insight into the relations between model-derived water storages and both climatic and anthro-
pogenic impacts by extracting spatio-temporal correlations between these inter-related data

169
170
171
172 sets. For a better spatial analysis of water storage and to reduce the uncertainty of estimations,
173 the study area is divided into six major areas: the eastern part of Iran (indicated by East),
174 Caspian Sea, Centre, Sarakhs, Persian Gulf and Oman Sea, and Lake Urmia (Figure 1).

175
176 The remainder of this study is structured as follows: Section 2 provides details on W3RA
177 model, remotely sensed datasets, and in-situ measurements used. In Section 3, data assimilation
178 filtering techniques, CCA algorithm, and the outline of our experimental setup are described.
179 Results are presented and discussed in Section 4 including the data assimilation performance
180 and analyzing the relationship between the model estimations, rainfall and NDVI through CCA.
181 Finally, the study is concluded in Section 5.
182
183
184
185
186

187 **FIGURE 1**

188
189
190 **2. Study area and data**

191
192 *2.1. Iran*

193
194 Located in an arid and semi-arid region, Iran experiences strong regional differences
195 in climate (Figure 1). Subtropical conditions are dominant over the northern part, but 90%
196 of the country has limited rainfall with extremely hot summers in the central and southern
197 coastal regions (Golian et al., 2015). Much of the west to northwest of Iran is located in high
198 plateaus and mountain ranges associated with strong temperature differences between winter
199 and summer. By contrast, the centre to southern parts are warm (cf. Figure 1) for most of
200 the year with mild winters and hot summers. Annual rainfall, the main source of freshwater in
201 Iran, varies from 50 mm in the deserts to 2275 mm in the northern part of the country (FAO,
202 2009). Only a fraction of the country receives enough rainfall for agriculture. A growing use
203 of irrigation for agricultural productions (Ardakani, 2009) and the increasing population (from
204 ~55 million in 1990 to ~80 million in 2015 Karamouzzian and Haghdoost, 2015), make water
205 availability an important issue across the country (Michel, 2017).
206
207
208
209
210
211
212
213

214 *2.2. W3RA hydrological model*

215
216 The present study uses the globally distributed World-Wide Water Resources Assess-
217 ment system (W3RA) model, run at $1^\circ \times 1^\circ$. W3RA, based on the Australian Water Resources
218 Assessment system (AWRA) model (version 0.5) developed in 2008 by the Commonwealth Sci-
219 entific and Industrial Research Organization (CSIRO) is a daily grid-distributed biophysical
220
221
222

225
226
227
228 model that simulates landscape water stored in the vegetation and soil systems (see details in
229 van Dijk, 2010). The model represent and forecast terrestrial water cycles (van Dijk, 2010; Ren-
230 zullo et al., 2014). W3RA does not consider anthropogenic effects (e.g., irrigation). Therefore,
231
232 by assimilating GRACE TWS, which integrates both natural and anthropogenic signals (e.g.,
233
234 Schumacher et al., 2018), we hope to constrain the model’s water storage simulations and in-
235
236 troduce the missing variations. Meteorological forcing data that is used here are minimum and
237
238 maximum temperature, down-welling short-wave radiation, and precipitation from the Prince-
239
240 ton University (Sheffield et al., 2006). The model contains effective soil parameters, water
241
242 holding capacity and soil evaporation, relating greenness and groundwater recession, and satu-
243
244 rated area to catchment characteristics parameters (van Dijk et al., 2013). This one-dimensional
245
246 grid-based water balance model represents the water balance of the soil, groundwater and sur-
247
248 face water stores in which each cell is modeled independently of its neighbors (van Dijk, 2010;
249
250 Renzullo et al., 2014). The model state, which is used for data assimilation (2002-2012), is com-
251
252 posed of W3RA storages of the top, shallow root and deep root soil layers, and groundwater
253
254 storage in an one-dimensional system (vertical variability).

255 2.2.1. *Satellite-derived observations*

256
257 We use monthly GRACE level 2 (L2) gravitational Stokes’ coefficients truncated up
258
259 to spherical harmonic degree and order 90 along with their full error information from 2002
260
261 to 2012 provided by the ITSG-Grace2016 gravity field model (Mayer-Gürr et al., 2014). The
262
263 monthly full error information of the Stokes’ coefficients is used to construct an observation error
264
265 covariance matrix for the GRACE TWS fields to be used for data assimilation (Schumacher et
266
267 al., 2016). Degree 1 of Stokes’ coefficients are replaced with those estimated by Swenson et al.
268
269 (2008) to account for the movement of the Earth’s center of mass. Degree 2 and order 0 (C20)
270
271 coefficients are replaced by those from Satellite Laser Ranging solutions due to unquantified
272
273 large uncertainties in this term (e.g., Cheng and Tapley, 2004; Chen et al., 2007). Afterward,
274
275 following Wahr et al. (1998), the L2 gravity fields is converted to gridded TWS fields with a
276
277 $1^\circ \times 1^\circ$ spatial resolution.

278
279 Correlated noise in data due to anisotropic spatial sampling, instrumental noise (K-band
280
ranging system and GPS), and temporal aliasing caused by the incomplete reduction of short-
term mass variations (Forootan et al., 2014b) can be reduced by smoothing filters (e.g., Kusche
et al., 2009). The application of smoothing, however, causes a spatial leakage problem that can

281
282
283
284 141 be problematic given that strong water resources of Tigris River and the Persian Gulf Basin can
285 142 affect GRACE signals, as leakage-in errors, over the northwest and south of Iran, respectively.
286
287 143 To tackle these errors, we use a Kernel Fourier Integration (KeFIn) filter, proposed by Khaki
288 144 et al. (2018b), which defines an efficient averaging kernel to improve GRACE TWS within
289
290 145 Iran. The KeFIn filtering method accounts for signal attenuations and leakage effects caused
291
292 146 by smoothing in a two step filtering scheme (see more details in Khaki et al., 2018b). Lastly,
293 147 in order to reach absolute TWS estimates (similar to W3RA), the mean TWS for the study
294
295 148 period is taken from W3RA and added to the GRACE TWS anomalies time series.

296 149 Furthermore, since W3RA does not simulate lake dynamics, one needs to account for the
297
298 150 existing surface water storage over the Lake Urmia before assimilation of the GRACE TWS
299
300 151 data. Water level height datasets from satellite radar altimetry of Jason-1 (260 cycles from
301
302 152 2002 to 2008) and Jason-2 (165 cycles from 2008 to 2012) are used to separate groundwater
303
304 153 and surface water storage from GRACE TWS (more details in Section 3.1.2). We use the ExtR
305
306 154 post-processing technique (Khaki et al., 2014, 2015) to retrack the data and improve water
307
308 155 level measurements, which are erroneous within inland waters. Filtered surface heights are
309
310 156 then used to create time series for virtual gauge stations over the Lake Urmia. These time
311
312 157 series are subsequently used to remove the contribution of surface water storage changes from
313
314 158 GRACE TWS data before implementing the proposed data assimilation (see also the procedure
315
316 159 in Forootan et al., 2014a).

317
318 160 Satellite-derived precipitation data of TRMM-3B43 products (TRMM, 2011) from the Trop-
319
320 161 ical Rainfall Measuring Mission Project (TRMM; version 7) is used to study rainfall variations.
321
322 162 We convert the gridded precipitation products provided with a $0.25^\circ \times 0.25^\circ$ spatial scale to
323
324 163 $1^\circ \times 1^\circ$ for the period between 2002 and 2012. In addition, we use Version 4 gridded daily
325
326 164 Normalized Difference Vegetation Index (NDVI) derived from the NOAA Climate Data Record
327
328 165 (CDR) between 2002 and 2012 to further investigate climatic impacts. This dataset is pro-
329
330 166 duced by the NASA Goddard Space Flight Center (GSFC) and the University of Maryland
331
332 167 with a $0.05^\circ \times 0.05^\circ$ spatial resolution. The datasets are rescaled to a $1^\circ \times 1^\circ$ spatial resolution.
333
334 168 A summary of the data sets and links to download the data are provided in Table 1.

328 169 *2.2.2. Temperature*

335
336 170 Monthly average temperature data for the temporal period of 2003 to 2012 is acquired
337
338 171 from Climatic Research Unit (CRU; Harris, 2008), which is used in CCA as a climate indicator.

337
338
339
340 172 This data is provided using more than 4000 weather stations distributed around the world.
341 173 For the sake of consistency with other data sets, the collected $0.5^\circ \times 0.5^\circ$ spatial scale data is
342
343 174 converted to $1^\circ \times 1^\circ$.

345 175 *2.3. In-situ data*

347 176 We use in-situ groundwater level data collected from 562 observation wells distributed
348 177 over the six drainage divisions of East, Caspian Sea, Centre, Sarakhs, Persian Gulf and Oman
349
350 178 Sea, and Lake Urmia water (cf. Figures 1) to compare them with our results. Datasets are
351
352 179 provided by the Iran Water Resources Management Company (IWRMC) and are categorized
353 180 based on Iran's six largest provinces on a yearly temporal scale presenting groundwater storage
354
355 181 changes for an entire aquifer (Forootan et al., 2014a). Figure 2 shows an annual increase in
356 182 groundwater extraction and the number of drilled wells for the entire country derived from
357
358 183 IWRMC data sets. The IWRMC volumetric groundwater change measurements are converted
359 184 to equivalent water height using the area of each aquifer. The area-averaged time series of
360
361 185 groundwater changes for each aquifer is then generated and used for evaluating the results. The
362 186 modified in-situ groundwater time series are compared separately to the average assimilation
363
364 187 results for the same aquifer. River water discharge, the number of bore holes, and average
365
366 188 water use for farming, industry, and urban use provided by IWRMC are also used in the CCA
367 189 process (see Section 3.2). Details of all the applied datasets, as well as the model are presented
368
369 190 in Table 1.

372 191 **FIGURE 2**

374 192 **TABLE 1**

377 192 **3. Method**

379 193 *3.1. Data assimilation*

381 194 *3.1.1. EnSRF filtering*

383 195 In order to assimilate GRACE data into the W3RA model, we use the Ensemble Square-
384 196 Root Filter (EnSRF) following Whitaker and Hamill (2002). EnSRF is an extended version
385
386 197 of traditional Ensemble Kalman Filter (EnKF) that does not require the observations to be
387
388 198 perturbed by introducing a new sampling scheme. Here, EnSRF is selected to avoid sampling
389
390
391
392

393 errors that can be reflected in the background covariance matrix especially in using a limited
394 number of ensembles (Whitaker and Hamill, 2002). Khaki et al. (2017a) showed that this
395 method is highly capable of assimilating GRACE TWS data into a hydrological model amongst
396 the most commonly used filters. EnSRF adopts a similar analysis step to the EnKF in the sense
397 that the analysis perturbations are computed from the forecast perturbations by updating each
398 ensemble perturbation with a Kalman-like update step. In the present study X consists of six
399 different water storages including top soil, shallow soil, and deep soil water, vegetation, snow,
400 and groundwater storages. Previous studies, e.g., Forootan et al. (2014a) and Tourian et al.
401 (2015), have investigated the surface water variations, specifically, in the Lake Urmia Basin
402 and the Caspian Sea as the major source of surface water storage changes in Iran. Therefore,
403 here, we only focus on the estimation of sub-surface compartments including groundwater and
404 soil moisture. The modified GRACE TWS data (see Section 2.2.1 for details) is then used to
405 update the above water compartments excluding surface storage.

406 The forecast model state, the integrated model state by a dynamical model for N times (N
407 is the ensemble number), is represented by $X^f = [X_1^f \dots X_N^f]$, where X_i^f ($i = 1 \dots N$) is the
408 i th ensemble (hereafter ‘f’ refers to forecast and ‘a’ represents analysis). The corresponding
409 model state forecast error covariance of P^f is defined by:

$$410 P^f = \frac{1}{N-1} \sum_{i=1}^N (X_i^f - \bar{X}^f)(X_i^f - \bar{X}^f)^T, \quad (1)$$

$$411 \bar{X}^f = \frac{1}{N} \sum_{i=1}^N (X_i^f). \quad (2)$$

412 The update stage in EnSRF contains two steps. First, it updates the ensemble-mean following,

$$413 \bar{X}^a = \bar{X}^f + K(y - H\bar{X}^f), \quad i = 1 \dots N, \quad (3)$$

$$414 K = P^f(H)^T(HP^f(H)^T + R)^{-1}, \quad (4)$$

415 where K is the Kalman gain, y is the observation vector. The transition matrix and the
416 observation covariance matrix are indicated by H and R , respectively. Next, EnSRF updates
417 the forecast ensemble of anomalies $A^f = [A_1^f \dots A_N^f]$ into the analysis ensemble deviation A^a .
418 A^f as the deviation of model state ensembles from the ensemble mean is derived from,

$$419 A_i^f = X_i^f - \bar{X}^f. \quad (5)$$

EnSRF exploits the serial formulation of the Kalman filter analysis step in which the observations are assimilated each at a time to compute the analysis perturbations that exactly match the Kalman filter covariance (Hoteit et al., 2008) using the modified gain (\tilde{K}) with,

$$A^a = (I - \tilde{K}H)A_i^f, \quad (6)$$

$$\alpha = \left(1 + \sqrt{\frac{R}{HP^fH^T + R}}\right)^{-1}, \quad (7)$$

where I is an identity matrix. More details on EnSRF can be found in Whitaker and Hamill (2002) and Tippett et al. (2003).

3.1.2. Assimilating GRACE TWS into W3RA

Monthly gridded GRACE TWS data are assimilated into W3RA to update the model states, a summation of model vertical water compartments (here soil moisture, vegetation biomass, snow, and groundwater). Note that no parameter adjustment is considered here and the observations are only used to constrain the system states. The monthly increment (i.e., the difference between the monthly averaged GRACE TWS and simulated TWS) can be added to each day of the current month, which guarantees that the update of the monthly mean is identical to the monthly mean of the daily updates. In practice, the differences between the predictions and the updated states are added as offsets to the state vectors at the last day of each month to generate the ensembles for the next month assimilation step. We use Monte Carlo sampling of multivariate normal distributions with the errors representing the standard deviations of the forcing sets (precipitation, temperature, and radiation) to generate an initial ensemble (Renzullo et al., 2014). The perturbed meteorological forcing datasets, then, are integrated forward with the model from 2000 to 2002 providing 72 sets of state vectors (as suggested by Oke et al., 2008) at the beginning of the study period.

An application of small ensemble size is problematic in ensemble data assimilation systems, as it can lead to filter divergent or inaccurate estimation (Tippett et al., 2003). Therefore, we apply ensemble inflation that uses a small coefficient factor (here 1.12; Anderson et al., 2001) to inflate prior ensemble deviation from the ensemble-mean and increases their variations (Anderson et al., 2007). Furthermore, the Local Analysis (LA) scheme (Evensen, 2003; Ott et al., 2004) is applied for localization. LA improves the assimilation procedure by restricting the

505 observations used for the covariance matrix computation to a spatially limited area (Khaki et al.,
506 2017c). As a result, only those measurements located within a certain distance from a grid point
507
508 249 have an impact on the updated states (Evensen, 2003; Ott et al., 2004). Different localization
509
510 250 lengths are tested and their results are assessed against in-situ groundwater measurements
511
512 251 (Section 2.3) to reach the best case scenario (i.e., 5° half-width used in this study).
513
514 252

515 As mentioned, it is necessary to remove surface water storages from GRACE TWS data over
516
517 253 Lake Urmia before data assimilation. For this purpose, following Forootan et al. (2014a) who
518
519 254 undertook water analysis over the same area, we use satellite altimetry time series over the lake
520
521 255 to derive surface water storage. The Global Land Data Assimilation System (GLDAS) outputs
522
523 256 of total column soil moisture, snow water equivalent, and vegetation biomass water storage as
524
525 257 well as water level variations from altimetry are used to estimate temporal and spatial patterns
526
527 258 of surface water storage using Independent Component Analysis (ICA). The extracted patterns
528
529 259 are then adjusted to GRACE TWS products using a least squares adjustment (LSA) procedure
530
531 260 (see details in Forootan et al., 2014a). The GRACE data after removing surface water storage
532
533 261 is used for the data assimilation process over Lake Urmia.
534
535 262

532 263 *3.2. Canonical Correlation Analysis (CCA)*

534 264 The present study applies Canonical Correlation Analysis (CCA) to find the linear
535
536 265 connection of two sets of multidimensional variables of predictor (x_c) and criterion (y_c) values.
537
538 266 CCA is selected here rather than simple correlation analysis due to its ability in establishing
539
540 267 the relationships between multiple intercorrelated variables. CCA extracts canonical coefficients
541
542 268 that represent common processes between two or more variables (Chang et al., 2013) using an
543
544 269 eigenvector decomposition that yields linear weights, known as canonical coefficients, which
545
546 270 describe maximum correlations between variables (see details in Steiger and Browne, 1984).
547
548 271 The combination of variables with the first canonical coefficient for each set has the highest
549
550 272 possible multiple correlations with the variables in the other set. CCA extracts canonical
551
552 273 coefficients u and v such that $X_c = x_c^T u$ and $Y_c = y_c^T v$ (X_c and Y_c are canonical variates)

561
562
563
564 274 possess a maximum correlation coefficient (Chang et al., 2013) using the following function,
565

$$\begin{aligned}
 566 \quad R &= \frac{E[X_c Y_c]}{\text{sqrt}(E[X_c^2]E[Y_c^2])} \\
 567 &= \frac{E[u^T x_c y_c^T v]}{\text{sqrt}(E[u^T x_c x_c^T u]E[v^T y_c y_c^T v])} \\
 568 &= \frac{u^T C_{x_c, y_c} v}{\text{sqrt}(u^T C_{x_c, x_c} u v^T C_{y_c, y_c} v)},
 \end{aligned}
 \tag{8}$$

573
574 275 where C_{x_c, x_c} and C_{y_c, y_c} are covariance matrices of x_c and y_c , respectively and the objective in
575
576 276 above function is to maximize the correlation R . We use an eigenvalue decomposition procedure
577
578 277 to find the linear weights producing canonical coefficients, which imply maximum possible
579
580 278 correlations (see details in Steiger and Browne, 1984). There are different canonical coefficients
581
582 279 within each set leading to different uncorrelated coefficients. Nevertheless, the combination
583
584 280 of variables with the first canonical coefficient for each set has the highest possible multiple
585
586 281 correlations with the variables in the other set.

587
588 282 Two scenarios are considered for prediction: (i) the predictor (x_c) contains time series
589
590 283 of both groundwater used for farming, industry, and human consumption from IWRMC and
591
592 284 climate-related variables of precipitation, NDVI, and temperature (provided by Harris, 2008),
593
594 285 and (ii) the predictor (x_c) includes only climate-related variables of precipitation, NDVI, and
595
596 286 temperature. This is done to explore the impact of each scenario on water variations. The
597
598 287 criterion (y_c) in both scenarios contains water storage (groundwater and soil moisture) and
599
600 288 discharge (from IWRMC) variations. By applying CCA, we establish the best combinations
601
602 289 between two sets of variables in two different cases. By comparing the results of these two
603
604 290 scenarios, we can investigate how water use and climate variabilities impact water storage
605
606 291 changes within Iran. Nevertheless, there are other effective components (e.g., large-scale ocean-
607
608 292 atmosphere phenomenon, evaporation, and droughts) on the water storage, which is difficult to
609
610 293 include all of them in the process. This CCA scheme, however, could provide an insight on the
611
612 294 connection between the above components. Table 2 summarizes the experiments undertaken
613
614 295 in this study. The corresponding research objectives and related sections that contain each
615
616 296 experiment's results are also listed in the table.

610
611
612
613
614
615
616
TABLE 2

617
618
619 **4. Results and discussion**
620

621
622 *4.1. Simulated assimilation*

623 In the following, we analyze the effect of various scenarios of observations on the as-
624 simulation. As mentioned earlier, GRACE TWS observations are used to update the sum of
625 soil moisture, vegetation, snow, and groundwater compartments at each grid cell. Thus, it is
626 important to investigate the distribution of the increments between these compartments, espe-
627 cially soil moisture and groundwater storage while the influence of the remaining storages (i.e.,
628 vegetation and snow) is negligible. In particular, we are interested in monitoring the impacts
629 of trends in observations time series on different water components. Schumacher et al. (2018)
630 showed that assimilating GRACE TWS data can improve model simulation of seasonality and
631 trend of TWS, as well as individual water storage components. This point is important be-
632 cause the largest part of GRACE TWS trends caused by groundwater variations that originate
633 from both natural and human-induced (e.g. water use) changes while soil moisture variations
634 generally follow climate pattern. Simulation experiments are undertaken to monitor how obser-
635 vations' variations, and particularly their trends are reflected in soil moisture and groundwater
636 estimates during assimilation.
637
638

639 To illustrate how GRACE data assimilation can improve model states, we perform a syn-
640 thetic study, in which arbitrary errors (uncertainty with different magnitudes) are assigned to
641 different model derived water storage states. We evaluate whether these states accurately re-
642 ceive increments from GRACE TWS. To this end, we introduce different uncertainties to model
643 states and test how these are transferred to the assimilation forecast steps (cf. Eqs. (3)-(4)).
644 Figure 3 shows the relationship between selected uncertainties of water states and their corre-
645 sponding weights in the (synthetic) assimilation. Based on this setup, six different scenarios are
646 considered to explore the impact of weights as the ratio of the assigned increment derived for
647 each storage state to the summation of all states. The results presented in Figure 3 indicate an
648 average influence of assimilating GRACE TWS data into W3RA over Iran between 2003 and
649 2013. In general, as theoretically expected, higher weight (i.e., larger increment) is assigned
650 to a variable with a smaller uncertainty. In other words, by assimilating GRACE TWS, the
651 model's water states with larger uncertainty receive larger increments, and this is reverse for
652 states with smaller uncertainty. These results approve the recent results of Schumacher et al.
653 (2018), who assimilate GRACE TWS data into WGHM model over Australia. Figure 3 also
654 shows that the average correlations between the individual estimated storage in each scenario
655
656
657
658
659
660
661
662
663
664
665
666
667
668
669
670
671
672

673
674
675
676 329 and the assimilated GRACE TWS. The correlations are calculated after removing seasonal ef-
677
678 330 fects on time series to focus on trends. It can be seen that larger correlations to the GRACE
679
680 331 TWS trends are obtained for a compartment with larger uncertainty and correspondingly with
681
682 332 a larger increment. This means that the assimilation process transfers the observation trends
683
684 333 into the more uncertain storage, which receives the larger corrections.

685 686 687 688 689 690 691 692 693 694 695 696 697 698 699 700 701 702 703 704 705 706 707 708 709 710 711 712 713 714 715 716 717 718 719 720 721 722 723 724 725 726 727 728

334 Another synthetic experiment is also implemented, where, different observation sets are
335
336 assimilated into W3RA but this time without manipulating their uncertainties. The aim is to
337
338 investigate whether the distribution of increments of different water states changes when the
339
340 TWS observations change. Here, four different synthetic observation scenarios are considered,
341
342 which include two versions of the WaterGAP Global Hydrology Model (WGHM; more details
343
344 on Döll et al., 2003; Müller et al., 2014) TWS estimates with and without water abstractions,
345
346 GRACE-derived TWS, and GRACE TWS minus WGHM soil moisture that roughly gives
347
348 groundwater observations. The spatially averaged time series of the TWS observations (for the
349
350 first three cases) over Iran are displayed in Figure 4a. The difference between the WGHM TWS
351
352 observations with and without water use clearly show the anthropogenic impacts as a distinct
353
354 negative trend in WGHM with water abstraction impact. A similar trend can also be seen in
355
356 GRACE TWS. Assimilation of these observations can show how water storages, for example
357
358 their trends, are distributed between soil moisture and groundwater estimates. Assimilating
359
360 WGHM TWS without water use, which does not show any significant trends, might better
361
362 estimate soil moisture. This is due to the fact that the main source of TWS's negative trends is
363
364 groundwater exploitation, while soil moisture variations generally are related to climatic (e.g.,
365
366 precipitation) variations. Hence, comparing the soil moisture results of assimilating GRACE
367
368 TWS and WGHM TWS with water use with those of WGHM TWS without water use can help
369
370 to assess the performance of data assimilation in updating soil moisture. Furthermore, while
371
372 the first three observation sets (i.e., WGHM with and without water use and GRACE-derived
373
374 TWS) are used to update the summation of all compartments, the last case (GRACE TWS
375
376 minus WGHM soil moisture) is used to update only the groundwater simulations. The main
377
378 rationale for updating only groundwater in the last experiment is to compare its results with
379
380 the other scenarios, which can help to investigate how accurate groundwater corrections are

729
730
731 applied from TWS increments in the other cases, where different compartments are available.
732
733

734 FIGURE 4

735
736
737 The results of the data assimilation variants are shown in Figures 4b and 4c and updated
738 groundwater estimates from assimilating GRACE TWS minus WGHM soil moisture is plotted
739 in Figure 4c. The assimilation results for soil moisture (Figure 4b) and groundwater (Figure
740 4c) show that the negative TWS trends are largely reflected only in groundwater time series.
741 The average correlation between the above TWS observations and corresponding groundwater
742 estimates is 0.92, 42% (on average) larger than for the open-loop run, which indicates the
743 suitability of data assimilation for constraining system states. For the entire area, there is
744 a stronger agreement between the soil moisture from assimilation compared to the open-loop
745 run, e.g., 22% (on average) for the GRACE TWS case and 28% (on average) for the WGHM
746 TWS with water use case. Lower correlations are obtained for assimilating WGHM TWS
747 without water use in comparison to other data assimilation scenarios (see also Figure 4b).
748 Furthermore, groundwater variations from the assimilated GRACE TWS are largely correlated
749 to the groundwater estimates from assimilating only groundwater observations (GRACE TWS
750 minus WGHM soil moisture). TWS observations of WGHM without water use have the least
751 effect on groundwater variations.
752
753
754
755
756
757
758
759

760 It can be concluded from Figure 4 that the data assimilation process successfully distributes
761 TWS increments between soil moisture and groundwater storages. These results indicate that
762 the largest part of increments during data assimilation is assigned to groundwater. The larger
763 impact on groundwater, based on Figure 3, suggests that the groundwater estimation of W3RA
764 is more uncertain than its soil moisture and as a result it receive larger updates. This is even
765 more clear in Figure 5, where groundwater and soil moisture estimates by ensemble members be-
766 tween 2004 and 2008 are shown. This time period is selected because it includes an episode with
767 strongly negative groundwater trend after 2005 (see also Figure 4c), where ensemble spreads
768 show a different pattern, e.g., larger spreads. The propagated groundwater ensemble members
769 are more dispersed than those of soil moisture, which causes larger ensemble deviations from its
770 mean and consequently larger uncertainty for the states (cf. Eqs. (1)-(2)). This can be due to
771 the point that the W3RA model has a simplified simulation of groundwater dynamics for un-
772 confined groundwater and does not simulate confined groundwater dynamics or anthropogenic
773
774
775
776
777
778
779
780
781
782
783
784

785
786
787
788 387 groundwater extraction (Tregoning et al., 2012). The larger corrections applied to groundwater
789 388 is also realistic considering the fact that a majority of water depletion in Iran occurs in ground-
790
791 389 water due to large extractions for irrigation. The applied irrigation water is likely to locally
792
793 390 increase total soil column water storage, which may contribute to a smaller decline in soil water
794
795 391 content (Michel, 2017).

796 797 798 799 800 801 802 803 804 805 806 807 808 809 810 811 812 813 814 815 816 817 818 819 820 821 822 823 824 825 826 827 828 829 830 831 832 833 834 835 836 837 838 839 840

392 Even though the results indicate good performance of GRACE data assimilation, one might
393 still expect artefacts from the TWS increments on the state estimates. The absence of ground-
394 water abstractions and anthropogenic impacts in most hydrological models, especially where
395 the rate of this extraction is high, can cause a misinterpretation of a negative TWS trend
396 captured by GRACE in the system states. As shown by Giroto et al. (2017), the assimila-
397 tion of GRACE TWS can successfully introduce the negative trends in the modeled TWS and
398 groundwater, however, this can also introduce unrealistic decline in other components, e.g., soil
399 moisture and evapotranspiration. This effect can be exacerbated when groundwater extraction
400 is large and occurs over an extended period. The model dynamical range of groundwater may
401 not be sufficient to accommodate the assimilated values (Zaitchik et al., 2008; Li and Rodell,
402 2015). Despite these, merging GRACE TWS data with high resolution models is the most ef-
403 ficient existing approach to analyze groundwater changes over wide areas, which in most cases
404 results in an improvement in the estimates (Li and Rodell, 2015; Giroto et al., 2017). Here,
405 we addressed this challenge by conducting a synthetic experiment, as well as by independently
406 assessing groundwater and soil moisture from assimilation. However, more investigations are
407 needed to be extended and the impacts of various data assimilation scenarios on each individual
408 water compartments need to be tested. These investigations are, however, out of the scope of
409 this study.

410 *4.2. Result evaluation*

411 In this section, we assess the performance of data assimilation using in-situ groundwater
412 measurements. To examine the validity of data assimilation results, in-situ groundwater mea-
413 surements of the six major drainage regions in the area including the East, Caspian Sea, Centre,
414 Sarakhs, Persian Gulf and Oman Sea, and Lake Urmia (cf. Figure 1) are used. For each basin in
415 Figure 1, we calculate the spatial average time series of groundwater storages with and without

841
842
843
844 416 data assimilation and compare them with the IWRMC in-situ and WGHM groundwater varia-
845 417 tion. We first analyze the performance of two assimilation cases of GRACE TWS and GRACE
846 418 TWS minus WGHM soil moisture data assimilation experiments for improving groundwater
848 419 estimates. Figure 6 shows the average root-mean-square error (RMSE) and standard deviation
849 420 (STD) calculated using groundwater from assimilation cases and in-situ measurements. Both
851 421 cases perform comparably in terms of RMSE and STD with an average of 38% error reduction
852 422 compared to open-loop. Nevertheless, assimilating GRACE TWS obtains the smaller RMSE
854 423 than groundwater only data assimilation. This further confirms the effectiveness of the applied
856 424 data assimilation for distribution TWS increments, especially for groundwater storage. Based
857 425 on this assessment, hereafter only the results for GRACE TWS data assimilation are presented.

860
861
862
863
864
865
866
867
868
869
870
871
872
873
874
875
876
877
878
879
880
881
882
883
884
885
886
887
888
889
890
891
892
893
894
895
896

FIGURE 6

426 The results for groundwater examination from data assimilation, WGHM, and the open-
427 loop run for each drainage division are illustrated in Figure 7, which show that the strongest
428 agreement between groundwater estimates and in-situ measurements occur in the assimilation
429 results. In most of the cases, WGHM performs better than the open-loop. For a better assess-
430 ment of data assimilation results, additional agreement statistics using RMSE and correlation
431 analysis are calculated and reported in Table 3. Significance at $p < 0.05$ was calculated using
432 the Students t-test with consideration of temporal autocorrelation through effective sample size.

FIGURE 7

TABLE 3

434 The computed time series for each region is compared to IWRMC data for the corresponding
435 region in order to estimate the reported statistics in Table 3. Generally, the assimilation results
436 are largely correlated with the in-situ data (0.85 on average) after data assimilation, with an
437 improvement of 35% over open-loop results. The largest improvements in terms of correlation
438 increase and RMSE reduction with respect to the in-situ measurements are achieved over Lake
439 Urmia, Sarakhs, and to a lesser degree Persian Gulf and Oman Sea. Table 3 shows considerable
440 groundwater decline in most of the regions especially within the Persian Gulf and Oman Sea
441 and Lake Urmia (both mostly located in the western areas). The largest negative groundwater

897
898
899
900 trend is exhibited for Lake Urmia while the lowest trend is found for the Caspian Sea division
901 in the north, which could be attributed to a large amount of precipitation in the latter region.

902 We further examine the soil moisture estimates from data assimilation. In the absence
903 of reliable in-situ soil moisture measurements over the study area, we use satellite-derived
904 and independent model soil moisture products. Soil moisture observations from the Advanced
905 Microwave Scanning Radiometer - Earth Observing System (AMSR-E) and Soil Moisture and
906 Ocean Salinity (SMOS) are compared to the assimilated top layer soil moisture estimates. The
907 motivation behind this comparison is based on the fact that SMOS and AMSR-E measurements
908 are largely correlated, respectively, to surface 0-5 cm and 0-2 cm soil moisture content (Njoku
909 et al., 2003). Figure 8 shows the average time series of the above comparison within the
910 study period. It can be seen that the assimilation top layer soil moisture is better matched
911 (41% improvement in correlation) to the satellite measurements in comparison to the open-loop
912 estimates. This shows a successful impact of GRACE TWS data assimilation on the model top
913 layer.
914
915
916
917
918
919
920
921
922

923 **FIGURE 8**

924
925 Total soil moisture estimates from data assimilation, i.e., summation of soil moisture at top,
926 shallow- and deep-root layers, are compared with soil moisture estimates of WGHM, the Global
927 Land Data Assimilation System (GLDAS; Rodell et al., 2004), and soil moisture provided by van
928 Dijk et al. (2014), who combined different data (e.g., GRACE) and model outputs (indicated
929 here as W3). The results are displayed in Figure 9. In all cases, data assimilation leads to a
930 better agreement to other products with an average 25% improvement. The largest correlation,
931 as well as the greatest improvement, are found for soil moisture after assimilation of WGHM.
932 There is also a considerable correlation between the results and W3.
933
934
935
936
937
938
939
940
941

942 **FIGURE 9**

943 *4.3. Water storage analysis*

944 Based on the improved soil moisture and groundwater estimates, spatio-temporal varia-
945 tions of both compartments are analyzed in this section. The variation of groundwater storages
946 within Iran before and after data assimilation are illustrated in Figure 10. The blue graph in
947 Figure 10 represents the average groundwater variations of all grid points after data assimi-
948 lation.
949
950
951
952

953
954
955
956 469 tion. This graph clearly shows a negative trend between 2002 and 2013 with an average -8.9
957 470 mm/year groundwater depletion for the entire country. However, such a trend is not present in
958 471 the open-loop time series. GRACE TWS data assimilation constrains groundwater estimates
960 472 and introduces this negative trend into the state as it exists in GRACE TWS observations (cf.
961 473 Figure 4). It is evident that the W3RA without data assimilation is not able to provide reli-
963 474 able long-term changes of groundwater, e.g., trend and multi-year variations. Therefore, data
965 475 assimilation is vital for reliable interpretation of ground water beyond the annual cycle. How-
966 476 ever, without additional information the data assimilation results cannot differentiate between
968 477 natural and anthropogenic causes. Apart from the trends, Figure 10 also shows a multi-year
969 478 cycle, e.g., positive trend between 2002 and 2005 and a stronger negative trend for the later
971 479 years 2006 to 2013. Again, this trend is not visible in the open-loop simulations.

974
975
976
977
978
979
980
981
982
983
984
985
986
987
988
989
990
991
992
993
994
995
996
997
998
999
1000
1001
1002
1003
1004
1005
1006
1007
1008

FIGURE 10

480 Furthermore, we separately analyze water compartments for each of Iran's major drainage
481 regions. The soil moisture and groundwater average time series from W3RA before and after
482 assimilating GRACE TWS for each of the divisions are shown in Figure 11 and Figure 12,
483 respectively. Larger soil moisture variations (in terms of amplitude) exist for the data assimi-
484 lation results compared to open-loop results in Figure 11. In particular, this is evident for the
485 Persian Gulf and Oman Sea and Caspian Sea. This could be due to a larger amount of annual
486 precipitation over these areas. Declines in soil water content can be seen in Sarakhs, especially
487 between 2005 and 2009, and Lake Urmia. In most of the regions, increases (e.g., large positive
488 variations) are observed during 2004 and 2010. Overall, better agreements between open-loop
489 and assimilation time series are found over East and Centre regions, where a semi-arid cli-
490 mate condition is dominant. GRACE data assimilation has the least impact on soil moisture
491 estimates within these areas.

FIGURE 11

492 Figure 12 depicts groundwater variations for each individual drainage division. Similar to
493 soil moisture analysis (cf. Figure 11), data assimilation results demonstrate larger magnitudes
494 than open-loop results. Except for the Caspian Sea, all the regions show a considerable decline
495 in groundwater estimates during the study period. In particular, this is clear in Lake Urmia,

1009
1010
1011
1012 496 Sarakhs, and Centre, especially after 2007. These trends are absent in the open-loop time series
1013 497 and derive from GRACE TWS after implementing data assimilation, which confirm the results
1014 498 shown in Figure 10. Larger groundwater declines are found in regions over the western parts
1015 499 of the country (e.g., the Persian Gulf and Oman Sea and Lake Urmia). In most of the cases,
1016 500 groundwater rise is observed as a positive trend between 2004 and 2005. These increases are
1017 501 then followed by consistent declines despite some short-term increases such as during 2010. A
1018 502 large trend decline is observed after 2006 in Lake Urmia, Centre, Sarakhs, and to a lesser degree
1019 503 in Caspian Sea. For the Persian Gulf and Oman Sea, Sarakhs, and Center, the groundwater
1020 504 negative trend is remarkable after 2008. Despite a small negative trend in East for the study
1021 505 period, the groundwater variations have the smallest amplitudes in this region compared to
1022 506 other areas. Seasonal variations can clearly be seen in most of the regions while this pattern is
1023 507 dominant mostly in Caspian Sea. Figure 12 and the reported negative trends in Table 3 show
1024 508 that groundwater depletion is a major issue in most parts of Iran resulting in a remarkable
1025 509 dryness across the country.

1033
1034
1035
1036
1037
1038
1039
1040
1041
1042
1043
1044
1045
1046
1047
1048
1049
1050
1051
1052
1053
1054
1055
1056
1057
1058
1059
1060
1061
1062
1063
1064

FIGURE 12

510 4.4. Climatic impacts

511 We further investigate the connection between climatic impacts and water storage vari-
512 ations. A comparison between groundwater and soil moisture variations and climate-related
513 variables such as precipitation and NDVI can reveal such interactions these parameters. Figure
514 13 shows maps of temporal average precipitation, soil moisture, and groundwater maps during
515 the study period. The first row in Figure 13 represent the average applied increment to soil
516 moisture and groundwater storages, the second row indicates variations (average of time series
517 at each grid point) of precipitation, soil moisture, and groundwater, and trends for each variable
518 at each grid point are depicted in the third row.

FIGURE 13

519 Figure 13 shows the spatial pattern of increments, i.e., the difference between assimilation
520 results and open-loop estimates, applied to the system states. It can be seen that the largest
521 increments are applied to groundwater storage as can be expected from Figures 3 and 4. These
522 corrections are mostly focused on the northwest to south and the eastern part of Iran. In soil

1065
1066
1067
1068 523 moisture, the increments can be found across the country, again, with larger concentrations
1069 524 in the western areas. The effect of data assimilation clearly can be seen by the increments
1070 525 illustrated in Figure 13. The spatial pattern of precipitation, soil moisture, and groundwater
1071 526 variations in Figure 13 show larger variations over the north toward northwest parts, where the
1072 527 Alborz mountain range cover a large portion of the areas. A similar pattern can also be seen
1073 528 in western parts, where the Zagros mountain range is located. Overall, the soil moisture map
1074 529 more closely reflects the precipitation patterns compared to groundwater variations, which can
1075 530 be attributed to impacts from water uses. Contrary to precipitation and soil moisture, negative
1076 531 groundwater variations are found over different regions, especially the north-western and south-
1077 532 ern parts. There are very limited variations in terms of amplitude changes for precipitation,
1078 533 soil moisture, and groundwater within the centre, eastern, and partially south-eastern parts of
1079 534 Iran. Trend maps (last row in Figure 13) illustrate spatial patterns for each component. Both
1080 535 precipitation and soil moisture show increasing trends in the north and to a lesser degree in
1081 536 the south. Groundwater trends are generally negative in all regions, but more strongly in the
1082 537 west, where Lake Urmia is located. A significant groundwater depletion can be observed in
1083 538 the central parts extended to the north, where Tehran, Iran's capital city is located. Large
1084 539 groundwater extractions in Tehran during the study period can be the main reason for this
1085 540 while in other areas, an excessive irrigation is a potential candidate for the observed depletion.
1086 541 It can be seen that there is an agreement between the applied increment by data assimilation,
1087 542 especially for groundwater, and the negative observed trends. Again it can be concluded that
1088 543 without using assimilation, these negative trends are not captured.

1100 544 To better quantify the spatio-temporal variations of water storage and climate variabilities,
1101 545 principal component analysis (PCA Lorenz, 1956) is applied on precipitation, NDVI, GRACE
1102 546 TWS, and groundwater time series. This allows us to monitor the relationship between the
1103 547 estimated groundwater and GRACE TWS, as well as their connection to climatic impacts
1104 548 through precipitation and NDVI. The first three extracted principal components (PC1, PC2,
1105 549 and PC3) of each component are plotted in Figure 14. There is good agreement between the
1106 550 time series for all three cases, in particular for seasonal variations. All time series in PC1
1107 551 show a clear annual variation. Negative trends, especially after 2009 are only captured by
1108 552 PC1 of GRACE TWS and groundwater. Stronger agreements between precipitation and NDVI
1109 553 PCs can be found. This can be attributed to vegetation growth response to rainfall and soil
1110 554 moisture. The assimilated groundwater storage variations largely follow the GRACE TWS

1121
1122
1123
1124 555 variation patterns, both in terms of variability and trend, mainly due to the application of
1125 556 GRACE data assimilation. Both of these variables are strongly correlated with rainfall time
1126
1127 557 series in PC2 and PC3 with an average correlation of 0.86. Various strong anomalies are occur in
1128
1129 558 the time series, e.g., in 2005 and 2010. Increases in the time series occur in PC1 for all variables
1130
1131 559 between 2004 and 2006 and during 2010 and 2012. PC2 shows similar rises in 2008 and 2010
1132
1133 560 followed by a strong decrease. PC3 shows an increase in 2009 and 2010 in the precipitation,
1134
1135 561 GRACE TWS, and groundwater which explains the corresponding increase in water storages
1136
1137 562 (cf. Figures 10 and 12). Some negative anomalies are found in PC3 in 2003, 2005, and 2011 and
1138
1139 563 also in 2006 and 2013. The other variables generally demonstrate the same variation pattern as
1140
1141 564 precipitation, which shows a strong connection between water storage variations and climatic
1142
1143 565 changes. Water storage variations in Iran, however, are also affected by non-climate factors
1144
1145 566 (e.g., anthropogenic impacts), which are likely the cause of the observed negative trends in
1146
1147 567 PC1 for GRACE TWS and groundwater.

1145 1146 1147 1148 1149 1150 1151 1152 1153 1154 1155 1156 1157 1158 1159 1160 1161 1162 1163 1164 1165 1166 1167 1168 1169 1170 1171 1172 1173 1174 1175 1176

568 The corresponding empirical orthogonal functions (EOF1, EOF2, and EOF3) extracted by
569 applying PCA on precipitation, NDVI, GRACE TWS, and groundwater from data assimilation
570 are shown in Figure 15. Overall, the mode 1 represents a strong annual signal (as would be
571 expected), mode 2 shows some deviations from the annual signal (e.g. inter-annual variations)
572 in the same regions as for mode 1. Mode 3 to some extent shows inter-annual variations but
573 importantly shows some extreme values. The spatial patterns of NDVI, GRACE TWS, and
574 groundwater are largely correlated to rainfall pattern, especially in EOF1 and EOF2. Larger
575 spatial variations exist over the northern and western parts of Iran, which seem to cause larger
576 water storage and NDVI changes in the same areas. These are the parts with higher altitudes
577 in which precipitation rates are generally high. GRACE TWS and groundwater EOF2 maps
578 show strong positive signals over the north toward the northwest and partially in western areas.
579 The rainfall EOF2 map, however, does not show a large signal over the north-western part but
580 only over the northern and western parts, where the Alborz and Zagros mountain ranges are
581 located. On the other hand, all variables show a negative signal in the south-eastern part.
582 Positive signals over the eastern parts, with smaller amplitudes, compared to EOF1 and EOF2
583 for NDVI, GRACE TWS, and groundwater are displayed by EOF3 maps. Negative signals can

1177
1178
1179
1180 be seen in EOF3 maps, especially for groundwater mostly over the northwestern areas, where
1181 Lake Urmia is located, as well as the northeast and Sarakh.
1182
1183

1184
1185
1186
1187
1188
1189
1190
1191
1192
1193
1194
1195
1196
1197
1198
1199
1200
1201
1202
1203
1204
1205
1206
1207
1208
1209
1210
1211
1212
1213
1214
1215
1216
1217
1218
1219
1220
1221
1222
1223
1224
1225
1226
1227
1228
1229
1230
1231
1232

FIGURE 15

586 4.5. CCA results

587 We further implement CCA on the estimated water compartments (from the data as-
588 simulation) on the one hand, and human- as well as climate-related variables on the other hand
589 in two different scenarios, i.e., (i) the predictor contains time series of both groundwater used
590 (e.g., for farming and industry) and climate-related variables (precipitation, NDVI, and tem-
591 perature), and (ii) the predictor includes only climate-related variables of precipitation, NDVI,
592 and temperature (cf. Section 3.2). By this, we can establish the relations between water stor-
593 ages and other factors. CCA is applied to the spatially averaged time series of all variables
594 to estimate canonical coefficients. Canonical loadings are used to interpret the CCA results,
595 which measure the simple linear correlation between an observed variable and the estimated
596 canonical variates (Dattalo, 2014). The interpretation is mostly based on examining the sign
597 and the magnitude of the canonical coefficients assigned to each variable. Variables with larger
598 coefficients contribute more to the variates and variables with opposite signs exhibit an inverse
599 relationship with each other while those with the same sign exhibit a direct relationship. De-
600 tailed results of the CCA experiment for each scenario applied within Iran are presented in
601 Table 4.

TABLE 4

602 The table summarizes the contribution of each variable in CCA. Results indicate that sce-
603 nario (i) leads to larger canonical correlation coefficients in comparison to scenario (ii). This
604 means that variations in water storages are more correlated to variations of the combined
605 human- and climate-related parameters. Note that CCA extract different sets of results (roots),
606 thus, we only use the first root that is statistically significant (for a significant level of 0.05). It
607 can be seen from Table 4 that the water use has strong negative correlations to water storage
608 variations, especially groundwater, which has the largest loading. This means that water con-
609 sumption for various uses (especially farming) is a very effective factor within the country that
610 causes the greatest impact on groundwater (with 0.938 canonical correlation). Among climate

1233 variables, precipitation, and to a lesser degree temperature have also a considerable influence
1234 on water storage variations. Not surprisingly, an increase (or decrease) in rainfall directly leads
1235 to increase (or decrease) in water storages as indicated by the same signs. Table 4 suggests that
1236 variations in groundwater use and climate parameters in both scenarios have minimum impact
1237 on water discharge. This may be due to the fact that surface waters compose a relatively small
1238 amount of water availability across Iran in comparison to other storages such as groundwater.
1239

1240 It can also be inferred from Table 4 that removing the water use from scenario (i) results
1241 in smaller canonical correlation in (ii), which means a smaller agreement between variables in
1242 scenario (ii) and water storage changes, even though this removal causes $\sim 3\%$ and 5% increase in
1243 loadings of precipitation and temperature, respectively. Comparing the results of both scenarios
1244 implies the large anthropogenic impact (more than climate-related factors) on water storages
1245 variations, which makes it essential to include this impact along with climatic effects while one
1246 studies sub-surface water storage variations in Iran. Figure 16 depicts scatter bi-plots and the
1247 linear trend which represents the correspondence between two sets of variables using average
1248 canonical coefficients for each scenario. It can be seen that the distribution of the two datasets
1249 in scenario (i) has smaller deviations and is more symmetric (closer to the reference line than
1250 scenario (ii)), which leads to higher canonical correlation for the first scenario. Figure 16 shows
1251 that incorporating the water use results in a better agreement between the criterion, i.e., water
1252 storage variations and predicant. This stresses the necessity of considering the water use and
1253 anthropogenic impacts (e.g., irrigation) on water storages analyzes, which cannot be happen
1254 without inclusion of GRACE TWS into the process.
1255
1256
1257
1258
1259
1260
1261
1262
1263
1264
1265
1266
1267
1268
1269

1270 **FIGURE 16**

1271 **5. Conclusions**

1272 Sub-surface water storages are a major source of freshwater in Iran. With increased
1273 population and irrigated land, water availability has become a serious issue across the country.
1274 In the present study we assimilate GRACE TWS into W3RA to separately analyze different
1275 water compartments including groundwater, soil moisture, and surface water storages. The
1276 six major drainage divisions in the area including the eastern part of Iran (East), Caspian
1277 Sea, Centre, Sarakhs, Persian Gulf and Oman Sea, and Lake Urmia are considered to better
1278 understand water availability in the different regions. An analysis is undertaken to examine the
1279
1280
1281
1282
1283
1284
1285
1286
1287
1288

1289
1290
1291 effects of GRACE data assimilation on different water storage compartments. It is found that
1292
1293 the implemented process can effectively distribute the TWS increments between groundwater
1294
1295 and soil moisture storages. Although the results show improvements in both groundwater and
1296
1297 soil moisture, the data assimilation still may have introduced some artefacts into the simulated
1298
1299 groundwater dynamics due to the massive effects of groundwater extraction within the country,
1300
1301 which requires an independent extensive study and more comprehensive analysis.

1302
1303 It is found that the application of GRACE TWS data assimilation can significantly improve
1304
1305 the performance of W3RA. Data assimilation successfully correct for the open-loop simulation
1306
1307 variations, e.g., in terms of trends and multi-year variations, especially for groundwater storage.
1308
1309 Based on the improved estimates, we find that groundwater trends in a large part of the
1310
1311 country's central, western and southern areas are negative representing a significant water
1312
1313 availability issue. An average -8.9 mm/year water storages decline is observed during 2002 to
1314
1315 2012 with a larger rate since 2005 suggesting that Iran is becoming considerably dryer. Larger
1316
1317 water store depletions are found to occur in the Persian Gulf and Oman Sea and Lake Urmia
1318
1319 with lesser effects on soil moisture in these regions. In the Caspian Sea region, however, due to
1320
1321 a large amount of precipitation, smaller groundwater and soil moisture trends are observed. In
1322
1323 the Persian Gulf and Oman Sea, -9.3 mm/year (on average) groundwater trend is found, which
1324
1325 is the second largest negative trend after that of Lake Urmia.

1326
1327 Furthermore, PCA is applied to investigate the relationship between the estimated ground-
1328
1329 water and GRACE TWS, as well as their connection to climatic impacts in various parts of
1330
1331 Iran. Larger water storage spatial variations are observed over the northern and western parts
1332
1333 of Iran with higher altitudes in which precipitation rates are generally high. Contrary to rainfall
1334
1335 maps, strong positive GRACE TWS and groundwater signals are found over the north toward
1336
1337 the northwest and partially in western areas. In terms of temporal variations, water storage
1338
1339 variables generally demonstrate the same variation pattern as precipitation, however, they are
1340
1341 also affected by non-climate factors (e.g., anthropogenic impacts), which are likely the cause of
1342
1343 the observed negative trends in GRACE TWS and groundwater time series. Therefore, CCA is
1344
1345 applied to explore the relationship between water storages estimated by data assimilation and
1346
1347 climatic, as well as anthropogenic indicators. The application of CCA reveals strong correla-
1348
1349 tion (0.89 in average) suggesting that the groundwater use has a major impact on water storage
1350
1351 variations.

1345
1346
1347
1348 **Acknowledgement**

1349
1350 M. Khaki is grateful for the research grant of Curtin International Postgraduate Research
1351 Scholarships (CIPRS)/ORD Scholarship provided by Curtin University (Australia). This work
1352
1353 is a TIGeR publication.
1354

1355
1356 **References**

1357
1358 Afshar, A.A., Joodaki, G.R., Sharifi, M.A. (2016). Evaluation of Groundwater Resources in
1359 Iran Using GRACE Gravity Satellite Data. JGST., 5 (4) :73-84, [http://jgst.issge.ir/article-](http://jgst.issge.ir/article-1-381-fa.html)
1360
1361 1-381-fa.html.
1362

1363 Amery, H.A., Wolf, A.T. (2000). Water in the Middle East: A Geography of Peace, University
1364 of Texas Press, Austin, Tex.
1365
1366

1367 Anderson, J. (2001). An Ensemble Adjustment Kalman Filter for Data As-
1368 simulation. Mon. Wea. Rev., 129, 2884-2903, [http://dx.doi.org/10.1175/1520-](http://dx.doi.org/10.1175/1520-0493(2001)129;2884:AEAKFF;2.0.CO;2)
1369
1370 0493(2001)129;2884:AEAKFF;2.0.CO;2.
1371

1372 Anderson, M.C., Norman, J.M., Mecikalski, J.R., Otkin, J.A., Kustas, W.P. (2007). A climato-
1373 logical study of evapotranspiration and moisture stress across the continental United States
1374 based on thermal remote sensing: 1. Model formulation. J. Geophys. Res. 112 (D10117).
1375
1376
1377 <http://dx.doi.org/10.1029/2006JD007506>.
1378

1379 Ardakani, R. (2009). Overview of water management in Iran. Proceeding of regional center on
1380 urban water management, Tehran, Iran.
1381
1382

1383 Bennett, A.F. (2002); Inverse Modeling of the Ocean and Atmosphere, 234 pp., Cambridge
1384 Univ. Press, New York.
1385
1386

1387 Bertino, L., Evensen G., Wackernagel, H. (2003). Sequential Data Assimilation Techniques in
1388 Oceanography, International Statistical Review, Vol. 71, No. 2, pp. 223-241.
1389
1390

1391 Chang, B., Kruger, U., Kustra, R., Zhang, J. (2013). Canonical Correlation Analysis based
1392 on Hilbert-Schmidt Independence Criterion and Centered Kernel Target Alignment, Volume
1393 28: Proceedings of The 30th International Conference on Machine Learning, 2, 28, 316-324,
1394
1395
1396 <http://jmlr.csail.mit.edu/proceedings/papers/v28/chang13.pdf>.
1397
1398
1399
1400

- 1401
1402
1403
1404 698 Chen, J.L., Wilson, C.R., Famiglietti, J.S., Rodell, M. (2007). Attenuation effect on seasonal
1405 699 basin-scale water storage changes from GRACE time-variable gravity. *Journal of Geodesy*,
1406 700 81, 4, 237245. <http://dx.doi.org/10.1007/s00190-006-0104-2>.
- 1408
1409 701 Chen, J.L., Wilson, C.R., Tapley, B.D. (2013). Contribution of ice sheet and mountain glacier
1410 702 melt to recent sea level rise. *Nat. Geosci.*, 6, 549552, <http://dx.doi.org/10.1038/ngeo1829>.
- 1412
1413 703 Cheng, M.K., Tapley, B.D. (2004). Variations in the Earth's oblateness during
1414 704 the past 28 years. *Journal of Geophysical Research, Solid Earth*, 109, B09402.
1415 705 <http://dx.doi.org/10.1029/2004JB003028>.
- 1417
1418 706 Coumou, D., Rahmstorf, S. (2012). A decade of weather extremes *Nat. Clim. Change*, 2 (7),
1419 707 pp. 16.
- 1421
1422 708 Dattalo, P. (2014). A demonstration of canonical correlation analysis with orthogonal rota-
1423 709 tion to facilitate interpretation. Unpublished manuscript, School of Social Work, Virginia
1424 710 Commonwealth University, Richmond, Virginia.
- 1426
1427 711 Döll, P., Kaspar, F., Lehner, B. (2003). A global hydrological model for deriving water avail-
1428 712 ability indicators: model tuning and validation, *J. Hydrol.*, 270, 105134.
- 1430
1431 713 Eicker, A., Schumacher, M., Kusche, J., Dll, P., Mller-Schmied, H., (2014). Calibration/data
1432 714 assimilation approach for integrating GRACE data into the WaterGAP global hydrology
1433 715 model (WGHM) using an ensemble Kalman filter: first results, *SurvGeophys*, 35(6):12851309.
1434 716 <http://dx.doi.org/10.1007/s10712-014-9309-8>.
- 1437
1438 717 Evensen, G. (2003). The ensemble Kalman filter: Theoretical formulation and practical imple-
1439 718 mentation, *Ocean Dynamics*, 53, 343367, <http://dx.doi.org/10.1007/s10236-003-0036-9>.
- 1441
1442 719 FAO (Food and Agriculture Organization of the United Nations)(2009). FAO water report, 34.
1443
- 1444 720 Fatolazadeh, F., Voosoghi, B., Naeeni, M.R. (2016). Wavelet and Gaussian Approaches
1445 721 for Estimation of Groundwater Variations Using GRACE Data. *Groundwater*, 54: 7481,
1446 722 <http://dx.doi.org/10.1111/gwat.12325>.
- 1448
1449 723 Forootan, E., Rietbroek, R., Kusche, J., Sharifi, M.A., Awange, J., Schmidt, M., Omondi,
1450 724 P., Famiglietti, J. (2014a). Separation of large scale water storage patterns over Iran using

- 1457
1458
1459 725 GRACE, altimetry and hydrological data. *Journal of Remote Sensing of Environment*, 140,
1460 580-595, <http://doi.org/10.1016/j.rse.2013.09.025>.
1461 726
1462
1463 727 Forootan, E., Didova, O., Schumacher, M., Kusche, J., Elsaka, B. (2014b). Comparisons of
1464 atmospheric mass variations derived from ECMWF reanalysis and operational fields, over
1465 728 2003 to 2011. *Journal of Geodesy*, 88, Pages 503-514, <http://dx.doi.org/10.1007/s00190-014->
1466 729 0696-x.
1467 730
1468
1469
1470 731 Forootan, E., Safari, A., Mostafaie, A., Schumacher, M., Delavar, M., Awange, J. (2017).
1471 Large-scale total water storage and water flux changes over the arid and semi-arid
1472 732 parts of the Middle East from GRACE and reanalysis products. *Surveys in Geophysics*,
1473 733 <http://dx.doi.org/10.1007/s10712-016-9403-1>.
1474 734
1475
1476
1477 735 Garner, T.W., Wolf, R.A., Spiro, R.W. , Thomsen, M.F. (1999). First attempt at assimilating
1478 736 data to constrain a magnetospheric model, *J. Geophys. Res.*, 104(A11), 25145-25152,
1479 737 <http://dx.doi.org/10.1029/1999JA900274>.
1480
1481
1482 738 Giroto, M., De Lannoy, G.J., Reichle, R.H., Rodell, M. (2016). Assimilation of gridded terres-
1483 739 trial water storage observations from GRACE into a land surface model. *Water Resources*
1484 740 *Research*, 52(5), 4164-4183.
1485
1486
1487
1488 741 Giroto, M., De Lannoy, G.J., Reichle, R.H., Rodell, M., Draper, C., Bhanja, S.N., Mukherjee,
1489 742 A. (2017). Benefits and Pitfalls of GRACE Data Assimilation: a Case Study of Terrestrial
1490 743 Water Storage Depletion in India. *Geophysical Research Letters*.
1491
1492
1493 744 Golian, S., Mazdiyasni, O., AghaKouchak, A. (2015). Trends in meteorological and agricultural
1494 745 droughts in Iran. *Theor Appl Climatol* (2015) 119:679688, <http://dx.doi.org/10.1007/s00704->
1495 746 014-1139-6.
1496
1497
1498
1499 747 Harris, I.C. (2008). Climatic Research Unit (CRU) time-series datasets of variations in
1500 748 climate with variations in other phenomena. NCAS British Atmospheric Data Cen-
1501 749 tre, date of citation, University of East Anglia Climatic Research Unit; Jones, P.D.,
1502 750 <http://catalogue.ceda.ac.uk/uuid/3f8944800cc48e1cbc29a5ee12d8542d>.
1503
1504
1505 751 Hoteit, I., Pham, D.T., Triantafyllou, G., Korres, G. (2008). A new approximate solution of
1506 752 the optimal nonlinear filter for data assimilation in meteorology and oceanography, *Monthly*
1507 753 *Weather Review*, 136, 317-334.
1508
1509
1510
1511
1512

- 1513
1514
1515
1516 754 Hoteit, I., Pham, D.T., Gharamti, M. E., Luo, X. (2015). Mitigating Observation Perturbation
1517 755 Sampling Errors in the Stochastic EnKF, *Monthly Weather Review*, 143:7, 2918-2936.
1518
1519 756 Huntington, T.G. (2006). Evidence for intensification of the global water cycle: Review and
1520 757 synthesis, *J. Hydrol.*,319(14), 8395, <http://dx.doi.org/10.1016/j.jhydrol.2005.07.003>.
1522
1523 758 Joodaki, G., Wahr, J., Swenson, S. (2014). Estimating the human contribution to groundwater
1524 759 depletion in the Middle East, from GRACE data, land surface models, and well observations,
1526 760 *Water Resour. Res.*, 50, 26792692, <http://dx.doi.org/10.1002/2013WR014633>.
1527
1528 761 Kalnay, E. (2003). *Atmospheric modelling, data assimilation and predictability*. Cam-
1529 762 bridge University Press. pp. xxii 341. ISBNs 0 521 79179 0, 0 521 79629 6,
1531 763 <http://dx.doi.org/10.1256/00359000360683511>.
1533
1534 764 Karamouzian, M., Haghdoost, A.K. (2015). Population control policies in Iran, *The*
1535 765 *Lancet*, Volume 385, Issue 9973, 2127 March 2015, Page 1071, ISSN 0140-6736,
1537 766 [https://doi.org/10.1016/S0140-6736\(15\)60596-7](https://doi.org/10.1016/S0140-6736(15)60596-7).
1538
1539 767 Khaki, M., Forootan, E., Sharifi, M.A. (2014). Satellite radar altimetry wave-
1540 768 form retracking over the Caspian Sea. *Int. J. Remote Sens.*, 35(17), 63296356,
1542 769 <http://dx.doi.org/10.1080/01431161.2014.951741>.
1544
1545 770 Khaki, M., Forootan, E., Sharifi, M.A., Awange, J., Kuhn, M., (2015). Improved grav-
1546 771 ity anomaly fields from retracked multimission satellite radar altimetry observations
1547 772 over the Persian Gulf and the Caspian Sea. *Geophys. J. Int.* 202 (3): 1522-1534,
1549 773 <http://dx.doi.org/10.1093/gji/ggv240>.
1551
1552 774 Khaki, M., Hoteit, I., Kuhn, M., Awange, J., Forootan, E., van Dijk, A.I.J.M., Schumacher,
1553 775 M., Pattiaratchi, C., (2017a). Assessing sequential data assimilation techniques for integrating
1554 776 GRACE data into a hydrological model, *Advances in Water Resources*, Volume 107, Pages
1556 777 301-316, ISSN 0309-1708, <http://dx.doi.org/10.1016/j.advwatres.2017.07.001>.
1557
1558 778 Khaki, M., Ait-El-Fquih, B., Hoteit, I., Forootan, E., Awange, J., Kuhn, M., (2017b). A
1560 779 Two-update Ensemble Kalman Filter for Land Hydrological Data Assimilation with an Un-
1562 780 certain Constraint, *Journal of Hydrology*, Available online 25 October 2017, ISSN 0022-1694,
1563 781 <https://doi.org/10.1016/j.jhydrol.2017.10.032>.
1564
1565
1566
1567
1568

- 1569
1570
1571
1572 782 Khaki, M., Schumacher, M., J., Forootan, Kuhn, M., Awange, E., van Dijk, A.I.J.M., (2017c).
1573 783 Accounting for Spatial Correlation Errors in the Assimilation of GRACE into Hydrological
1574 784 Models through localization, *Advances in Water Resources*, Available online 1 August 2017,
1575 785 ISSN 0309-1708, <https://doi.org/10.1016/j.advwatres.2017.07.024>.
- 1578
1579 786 Khaki, M., Forootan, E., Kuhn, M., Awange, J., Papa, F., Shum, C.K., (2018a). A Study of
1580 787 Bangladesh's Sub-surface Water Storages Using Satellite Products and Data Assimilation
1581 788 Scheme, *Science of The Total Environment*, Volume 625, 2018, Pages 963-977, ISSN 0048-
1582 789 9697, <https://doi.org/10.1016/j.scitotenv.2017.12.289>.
- 1585
1586 790 Khaki, M., Forootan, E., Kuhn, M., Awange, J., Longuevergne, L., Wada, W., (2018b). Efficient
1587 791 Basin Scale Filtering of GRACE Satellite Products, In *Remote Sensing of Environment*,
1588 792 Volume 204, Pages 76-93, ISSN 0034-4257, <https://doi.org/10.1016/j.rse.2017.10.040>.
- 1590
1591 793 Knapp, T.R. (1978). Canonical correlation analysis: A general parametric significance-testing
1592 794 system. *Psychological Bulletin*. 85 (2): 410-416. <http://dx.doi.org/10.1037/0033-2909.85.2.410>
- 1594
1595 795 Kusche, J., Schmidt R., Petrovic, S., Rietbroek, R. (2009). Decorrelated GRACE time-variable
1596 796 gravity solutions by GFZ and their validation using a hydrological model, *Journal of Geodesy*,
1597 797 DOI 10.1007/s00190-009-0308-3.
- 1600
1601 798 Lahoz, W.A., Geer, A.J., Bekki, S., Bormann, N., Ceccherini, S., Elbern, H., Errera, Q., Eskes,
1602 799 H.J., Fonteyn, D., Jackson, D.R., Khatatov, B. (2007). The Assimilation of Envisat data
1603 800 (ASSET) project, *Atmos. Chem. Phys.*, 7, 1773 - 1796.
- 1605
1606 801 Li, B., Rodell, M. (2015). Evaluation of a model-based groundwater drought indicator in the
1607 802 conterminous US. *Journal of Hydrology*, 526, 78-88.
- 1609
1610 803 Lorenz, E. (1956). Empirical orthogonal function and statistical weather prediction. Technical
1611 804 Report Science Report No 1, Statistical Forecasting Project. MIT, Cambridge.
- 1613
1614 805 Madani, K. (2014). Water management in Iran: what is causing the looming crisis? *J Environ*
1615 806 *Stud Sci.* doi:10.1007/s13412-014-0182-z.
- 1617
1618 807 Mayer-Gürr, T., Zehentner, N., Klinger, B., Kvas, A. (2014). ITSG-Grace2014: a new GRACE
1619 808 gravity field release computed in Graz. - in: GRACE Science Team Meeting (GSTM), Pots-
1620 809 dam am: 29.09.2014.

- 1625
1626
1627
1628 810 Michel, D. (2017). Iran's impending water crisis. In *Water, Security, and US Policy*, edited by
1629 811 David Reed. 438 pages, ISBN-10:1138051519.
- 1630
1631 812 Mohammadi-Ghaleni, M., Ebrahimi, K. (2011). Assessing impact of irrigation and drainage
1632 813 network on surface and groundwater resources Case study: Saveh Plain, Iran, ICID 21st
1633 814 International Congress on Irrigation and Drainage, 1523 October 2011, Tehran, Iran.
- 1634
1635
1636 815 Motagh, M., Walter, T.R., Sharifi, M.A., Fielding, E., Schenk, A., Anderssohn, J., et al. (2008).
1637 816 Land subsidence in Iran caused by widespread water reservoir overexploitation. *Geophysical*
1638 817 *Research Letters*, 35, L16403. <http://dx.doi.org/10.1029/2008GL033814>.
- 1639
1640
1641 818 Müller Schmied, H., S. Eisner, D. Franz, M. Wattenbach, F. Portmann, M. Flrke, and P. Dll
1642 819 (2014), Sensitivity of simulated global-scale freshwater fluxes and storages to input data,
1643 820 hydrological model structure, human water use and calibration, *Hydrol. Earth. Syst. Sci.*, 18,
1644 821 35113538, <http://dx.doi.org/10.5194/hess-18-3511-2014>.
- 1645
1646
1647 822 Munier, S., Aires, F., Schlaffe, S., Prigent, C., Papa, F., Maisongrande, P., Pan, M. (2014).
1648 823 Combining data sets of satellite-retrieved products for basin-scale water balance study: 2.
1649 824 Evaluation on the Mississippi Basin and closure correction model. *Journal of Geophysical*
1650 825 *Research: Atmospheres*, 119, 12,100-12,116, <http://dx.doi.org/10.1002/2014JD021953>.
- 1651
1652
1653 826 Njoku, E.G. et al. (2003). Soil moisture retrieval from AMSR-e. *IEEE Transactions on Geo-*
1654 827 *science and Remote Sensing*. 41:2, 215-229.
- 1655
1656
1657 828 Ott, E., Hunt, B.R., Szunyogh, I., Zimin, A.V., Kostelich, E.J., Corazza, M., Kalnay, E., Patil,
1658 829 D.J., Yorke, J.A. (2004). A local ensemble Kalman Filter for atmospheric data assimilation.
1659 830 *Tellus*, 56A: 415-428.
- 1660
1661
1662 831 Oke, P.R., Brassington, G.B., Griffin, D.A., Schiller, A. (2008). The Bluelink Ocean
1663 832 Data Assimilation System (BODAS). *Ocean Modelling*, 21, 4670, [http://dx.doi.org/](http://dx.doi.org/10.1016/j.ocemod.2007.11.002)
1664 833 [10.1016/j.ocemod.2007.11.002](http://dx.doi.org/10.1016/j.ocemod.2007.11.002).
- 1665
1666
1667 834 Reager, J.T., Thomas, A.C., Sproles, E.A., Rodell, M., Beaudoin, H.K., Li, B., Famiglietti, J.S.
1668 835 (2015). Assimilation of GRACE Terrestrial Water Storage Observations into a Land Surface
1669 836 Model for the Assessment of Regional Flood Potential. *Remote Sens.* 2015, 7, 14663-14679.
- 1670
1671
1672 837 Renzullo, L.J., Van Dijk, A.I.J.M., Perraud, J.M., Collins, D., Henderson, B., Jin, H., Smith,
1673 838 A.B., McJannet, D.L. (2014). Continental satellite soil moisture data assimilation improves
1674
1675
1676
1677
1678
1679
1680

- 1681
1682
1683
1684 839 root-zone moisture analysis for water resources assessment. *J. Hydrol.*, 519, 27472762.
1685 840 <http://dx.doi.org/10.1016/j.jhydrol.2014.08.008>.
- 1687 841 Rodell, M., Houser, P. R., Jambor, U., Gottschalck, J., Mitchell, K., Meng, C. J., Arsenault,
1688 842 K., Cosgrove, B., Radakovich, J., Bosilovich, M., Entin, J. K., Walker, J. P., Lohmann, D.,
1689 843 Toll, D. (2004). The global land data assimilation system. *American Meteorological Society*,
1690 844 85, 3, 381-394. <http://dx.doi.org/10.1175/BAMS-85-3-381>.
- 1694 845 Sarraf, M., Owaygen, M., Ruta, G., Croitoru, L. (2005). Islamic Republic of Iran: Cost assess-
1695 846 ment of environmental degradation. Tech. Rep. 32043-IR. Washington, D.C.: World Bank.
- 1697 847 Schmidt, R., Petrovic, S., Gntner, A., Barthelmes, F., Wnsch, J., Kusche, J. (2008). Periodic
1698 848 components of water storage changes from GRACE and global hydrology models. *J. Geophys.*
1699 849 *Res.*, 113, B08419, <http://dx.doi.org/10.1029/2007JB005363>.
- 1703 850 Schumacher, M., Kusche, J., Döll, P. (2016). A systematic impact assessment of GRACE
1704 851 error correlation on data assimilation in hydrological models, *Journal of Geodesy*,
1705 852 <http://dx.doi.org/10.1007/s00190-016-0892-y>.
- 1708 853 Schumacher, M., Forootan, E., van Dijk, A.I.J.M., Mller Schmied, H., Crosbie, R.S., Kusche,
1709 854 J., Dll, P. (2018). Improving drought simulations within the Murray-Darling Basin by
1710 855 combined calibration/assimilation of GRACE data into the WaterGAP Global Hydrology
1711 856 Model, *Remote Sensing of Environment*, Volume 204, 2018, Pages 212-228, ISSN 0034-4257,
1712 857 <https://doi.org/10.1016/j.rse.2017.10.029>.
- 1717 858 Schunk, R.W., Scherliess, L., Sojka, J.J., Thompson, D.C. (2004). USU global ionospheric data
1718 859 assimilation models, *Atmospheric and Environmental Remote Sensing Data Processing and*
1719 860 *Utilization: an End-to-End System Perspective*, (ed. H.-L. A. Huang and H. J. Bloom), *Proc.*
1720 861 *of SPIE*, 5548, <http://dx.doi.org/10.1117/12.562448>, 327-336.
- 1723 862 Sheffield, J., Goteti, G., Wood, E.F. (2006). Development of a 50-yearhigh-resolution global
1724 863 dataset of meteorological forcings for land surfacemodeling, *J. Clim.*, 19(13), 30883111.
- 1727 864 Steiger, J.H., Browne, M.W. (1984). The comparison of interdependent correlations between
1728 865 optimal linear composites. *Psychometrika*, 49, 1121.
- 1730 866 Stewart, L.M., Dance, S.L., Nichols, N.K. (2008). Correlated observation errors in data assim-
1731 867 ilation. *Int. J. Numer. Meth. Fluids*, 56: 15211527. <http://dx.doi.org/10.1002/fld.1636>.

- 1737
1738
1739
1740 868 Swenson, S., Chambers, D., Wahr, J. (2008). Estimating geocentervariations from a combi-
1741 869 nation of GRACE and ocean model output. *Journal of Geophysical research*, 113, B08410,
1742 870 <http://dx.doi.org/10.1029/2007JB005338>.
- 1744
1745 871 Tangdamrongsub, N., Steele-Dunne, S.C., Gunter, B.C., Ditmar, P.G., and Weerts, A.H.
1746 872 (2015). Data assimilation of GRACE terrestrial water storage estimates into a regional
1747 873 hydrological model of the Rhine River basin, *Hydrol. Earth Syst. Sci.*, 19, 2079-2100,
1748 874 <http://dx.doi.org/10.5194/hess-19-2079-2015>.
- 1751
1752 875 Tapley, B.D., Bettadpur, S., Watkins, M., Reigber, C. (2004). The gravity recovery and climate
1753 876 experiment: mission overview and early results, *Geophysical Research Letters*, 31, L09607,
1754 877 doi: 10.1029/2004GL019920.
- 1757
1758 878 Tippett, M.K., Anderson, J.L., Bishop, C.H., Hamill, T.M., Whitaker, J.S. (2003). Ensemble
1759 879 square root filters, *Mon. Weath. Rev.*, 131, 148590.
- 1760
1761 880 Tourian, M.J., Elmi, O., Chen, Q., Devaraju, B., Roohi, Sh., Sneeuw, N. (2015). A space-
1762 881 borne multisensor approach to monitor the desiccation of Lake Urmia in Iran, *Remote*
1763 882 *Sensing of Environment*, Volume 156, January 2015, Pages 349-360, ISSN 0034-4257,
1764 883 <https://doi.org/10.1016/j.rse.2014.10.006>.
- 1767
1768 884 Tregoning, P., McClusky, S., van Dijk, A.I.J.M., Crosbie, R.S., Pea-Arancibia, J.L. (2012).
1769 885 Assessment of GRACE satellites for groundwater estimation in Australia, *Waterlines report*,
1770 886 National Water Commission, Canberra.
- 1773
1774 887 Trigo, R.M., Gouveia, C.M., Barriopedro, D. (2010). The intense 20072009 drought in the
1775 888 Fertile Crescent: Impact and associated atmospheric circulation, *Agric. For. Meteorol.*, 150,
1776 889 12451257.
- 1778
1779 890 Tropical Rainfall Measuring Mission (TRMM), (2011). TRMM (TMPA/3B43) Rainfall Es-
1780 891 timate L3 1 month 0.25 degree x 0.25 degree V7, Greenbelt, MD, Goddard Earth Sci-
1781 892 ences Data and Information Services Center (GES DISC), Accessed [Data Access Date]
1782 893 https://disc.gsfc.nasa.gov/datacollection/TRMM_3B43_7.html.
- 1785
1786 894 United Nations (2015). United Nations Department of Economic and Social Affairs. World
1787 895 Population Prospects: The 2015 Revision.

- 1793
1794
1795
1796
1797
1798
1799
1800
1801
1802
1803
1804
1805
1806
1807
1808
1809
1810
1811
1812
1813
1814
1815
1816
1817
1818
1819
1820
1821
1822
1823
1824
1825
1826
1827
1828
1829
1830
1831
1832
1833
1834
1835
1836
1837
1838
1839
1840
1841
1842
1843
1844
1845
1846
1847
1848
- 896 Van Camp, M., Radfar, M., Martens, K., Walraevens, K. (2012). Analysis of the groundwater
897 resource decline in an intramountain aquifer system in Central Iran. *Geologica Belgica*, 15/3,
898 176180.
- 899 van Dijk, A.I.J.M. (2010). The Australian Water Resources Assessment System: Technical
900 Report 3, Landscape model (version 0.5) Technical Description, CSIRO: Water for a Healthy
901 Country National Research Flagship.
- 902 van Dijk, A.I.J.M., Renzullo, L.J., and Rodell, M. (2011). Use of Gravity Recovery and
903 Climate Experiment terrestrial water storage retrievals to evaluate model estimates by
904 the Australian water resources assessment system, *Water Resour. Res.*, 47, W11524,
905 <http://dx.doi.org/10.1029/2011WR010714>.
- 906 van Dijk, A.I.J.M., Pea-Arancibia, J.L., Wood, E.F., Sheffield, J., Beck, H.E. (2013). Global
907 analysis of seasonal streamflow predictability using an ensemble prediction system and
908 observations from 6192 small catchments worldwide, *Water Resour. Res.*, 49, 27292746,
909 <http://dx.doi.org/10.1002/wrcr.20251>.
- 910 van Dijk, A.I.J.M., Renzullo, L.J., Wada, Y., Tregoning, P. (2014). A global water cycle reanal-
911 ysis (20032012) merging satellite gravimetry and altimetry observations with a hydrological
912 multi-model ensemble. *Hydrol Earth Syst Sci* 18:29552973, [http://dx.doi.org/10.5194/hess-](http://dx.doi.org/10.5194/hess-18-2955-2014)
913 18-2955-2014.
- 914 Voss, K.A., Famiglietti, J.S., Lo, M.-H., de Linage, C., Rodell, M., Swenson, S.C. (2013).
915 Groundwater depletion in the Middle East from GRACE with implications for transboundary
916 water management in the TigrisEuphratesWestern Iran region. *Water Resources Research*,
917 49, <http://dx.doi.org/10.1002/wrcr.20078>.
- 918 Vrugt, J.A., ter Braak, C.J.F., Diks, C.G.H., Schoups, G. (2013). Advancing hydrologic data
919 assimilation using particle Markov chain Monte Carlo simulation: theory, concepts and
920 applications, *Advances in Water Resources*, Anniversary Issue - 35 Years, 51, 457-478,
921 <http://dx.doi.org/10.1016/j.advwatres.2012.04.002>.
- 922 Wahr, J.M., Molenaar, M., Bryan, F. (1998). Time variability of the Earth's gravity field:
923 hydrological and oceanic effects and their possible detection using GRACE. *J Geophys Res*
924 108(B12):3020530229, <http://dx.doi.org/10.1029/98JB02844>.

1849
1850
1851
1852 925 Whitaker, J.S., Hamill, T.M. (2002). Ensemble data assimilation without perturbed observa-
1853 926 tions, *Mon. Wea. Rev.*, 130, 1913-1924.
1854
1855 927 Wolf, A.T., Newton, J.T. (2007). Case study transboundary dispute resolution: The Tigris-
1856 928 Euphrates Basin, Transboundary Freshwater Dispute Database (TFDD), Oregon State Uni-
1858 929 versity, <http://www.transboundarywaters.orst.edu/>.
1859
1860 930 Zaitchik, B.F., Rodell, M., Reichle, R.H. (2008). Assimilation of GRACE terrestrial water stor-
1862 931 age data into a land surface model: results for the Mississippi River Basin. *J Hydrometeorol*
1863 932 9(3):535-548, <http://dx.doi.org/10.1175/2007JHM951.1>.
1864
1865
1866
1867
1868
1869
1870
1871
1872
1873
1874
1875
1876
1877
1878
1879
1880
1881
1882
1883
1884
1885
1886
1887
1888
1889
1890
1891
1892
1893
1894
1895
1896
1897
1898
1899
1900
1901
1902
1903
1904

1905
1906
1907
1908
1909
1910
1911
1912
1913
1914
1915
1916
1917
1918
1919
1920
1921
1922
1923
1924
1925
1926
1927
1928
1929
1930
1931
1932
1933
1934
1935
1936
1937
1938
1939
1940
1941
1942
1943
1944
1945
1946
1947
1948
1949
1950
1951
1952
1953
1954
1955
1956
1957
1958
1959
1960

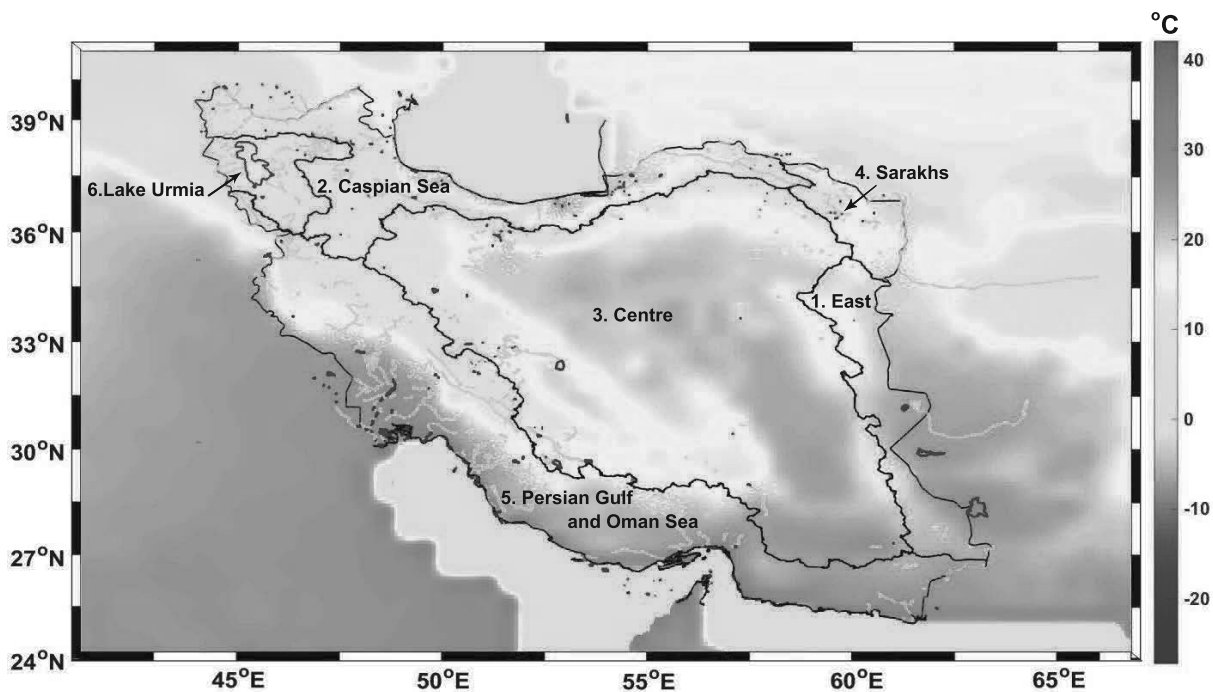


Figure 1: The study area and its average temperature (Harris, 2008). The figure also contains the locations of 6 major catchments separated by black solid lines.

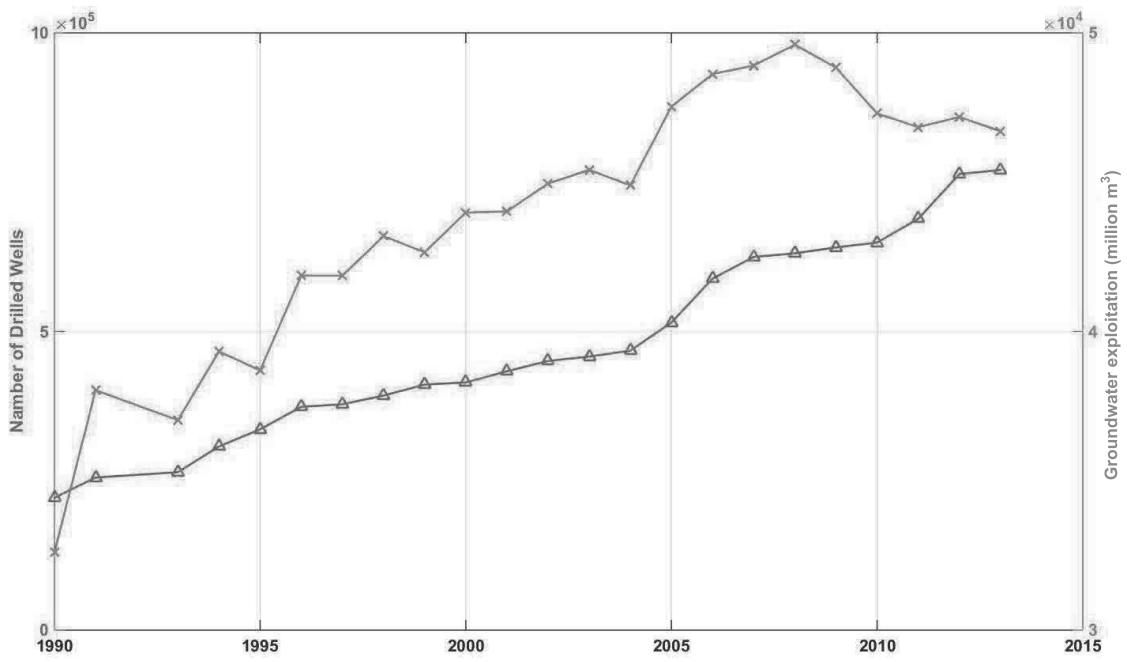


Figure 2: Groundwater depletion and the number of drilled wells in Iran from IWRMC.

2017
 2018
 2019
 2020
 2021
 2022
 2023
 2024
 2025
 2026
 2027
 2028
 2029
 2030
 2031
 2032
 2033
 2034
 2035
 2036
 2037
 2038
 2039
 2040
 2041
 2042
 2043
 2044
 2045
 2046
 2047
 2048
 2049
 2050
 2051
 2052
 2053
 2054
 2055
 2056
 2057
 2058
 2059
 2060
 2061
 2062
 2063
 2064
 2065
 2066
 2067
 2068
 2069
 2070
 2071
 2072

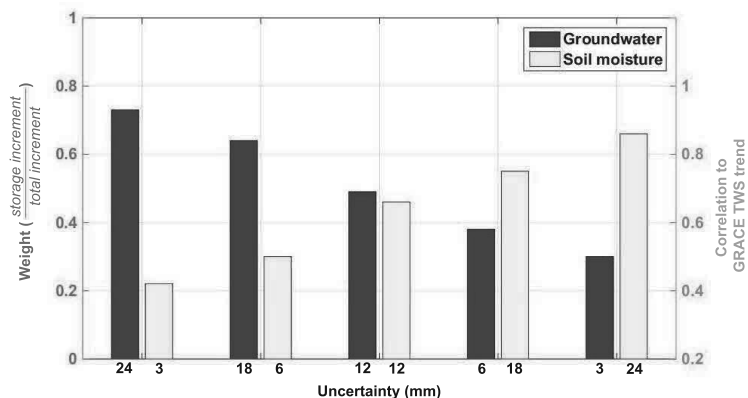


Figure 3: Relationships between groundwater and soil moisture state variable uncertainties and corresponding weights during data assimilation.

2073
2074
2075
2076
2077
2078
2079
2080
2081
2082
2083
2084
2085
2086
2087
2088
2089
2090
2091
2092
2093
2094
2095
2096
2097
2098
2099
2100
2101
2102
2103
2104
2105
2106
2107
2108
2109
2110
2111
2112
2113
2114
2115
2116
2117
2118
2119
2120
2121
2122
2123
2124
2125
2126
2127
2128

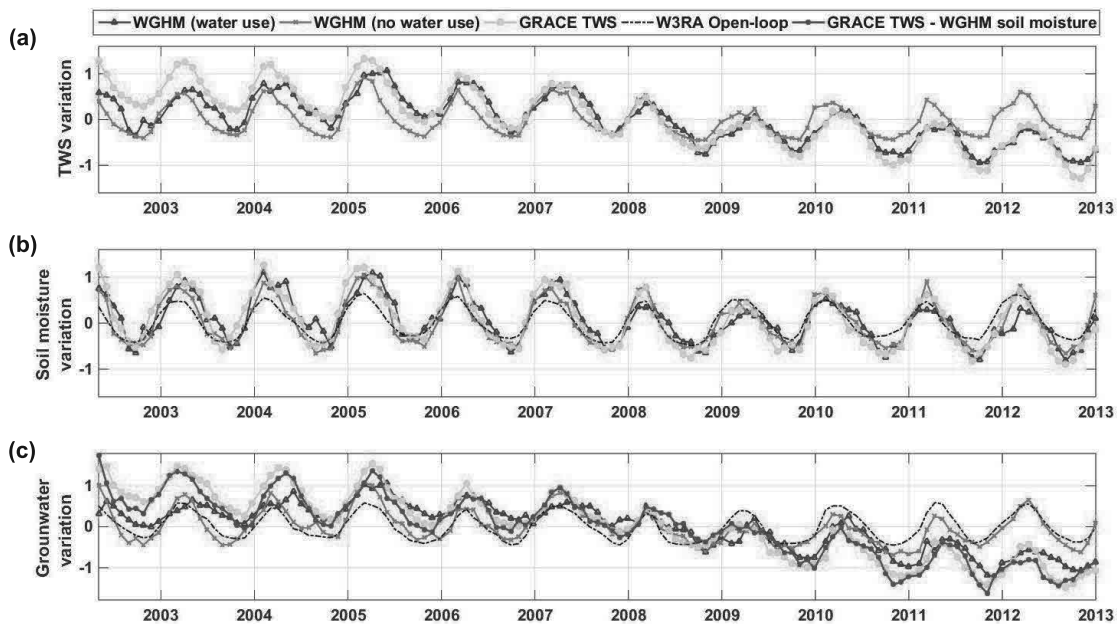


Figure 4: (a) Simulated average TWS observations using WGHM with and without human use, and W3RA open-loop plus GRACE trend. Average soil moisture (b) and groundwater (c) estimates from data assimilation based on simulated observations in (a).

2129
2130
2131
2132
2133
2134
2135
2136
2137
2138
2139
2140
2141
2142
2143
2144
2145
2146
2147
2148
2149
2150
2151
2152
2153
2154
2155
2156
2157
2158
2159
2160
2161
2162
2163
2164
2165
2166
2167
2168
2169
2170
2171
2172
2173
2174
2175
2176
2177
2178
2179
2180
2181
2182
2183
2184

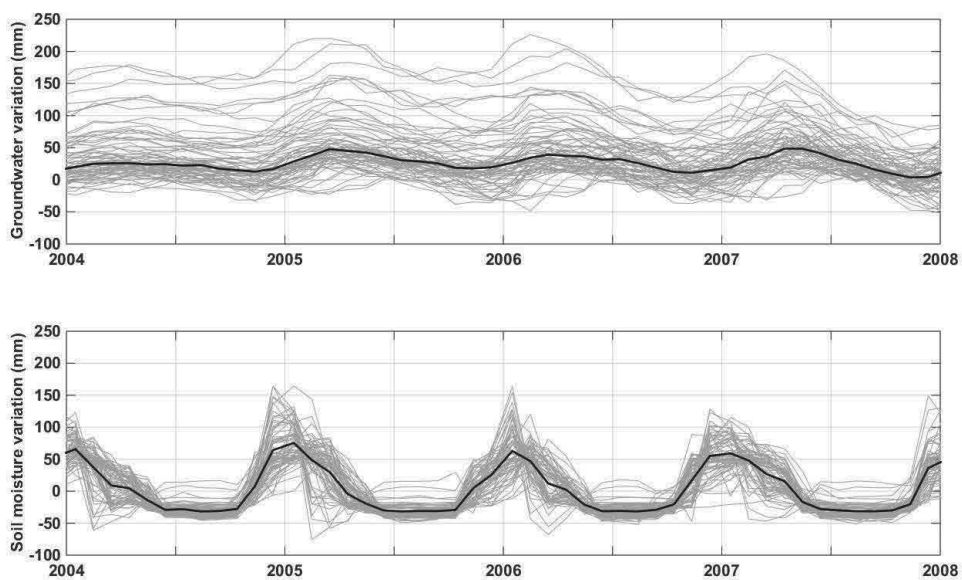


Figure 5: Average groundwater and soil moisture ensemble spreads between 2004 and 2008 over Iran. Gray lines indicate ensemble members and the black solid line present ensemble mean. Larger ensemble propagation is evident compared to that of soil moisture that represents larger uncertainties in the former water storage compartment.

2185
2186
2187
2188
2189
2190
2191
2192
2193
2194
2195
2196
2197
2198
2199
2200
2201
2202
2203
2204
2205
2206
2207
2208
2209
2210
2211
2212
2213
2214
2215
2216
2217
2218
2219
2220
2221
2222
2223
2224
2225
2226
2227
2228
2229
2230
2231
2232
2233
2234
2235
2236
2237
2238
2239
2240

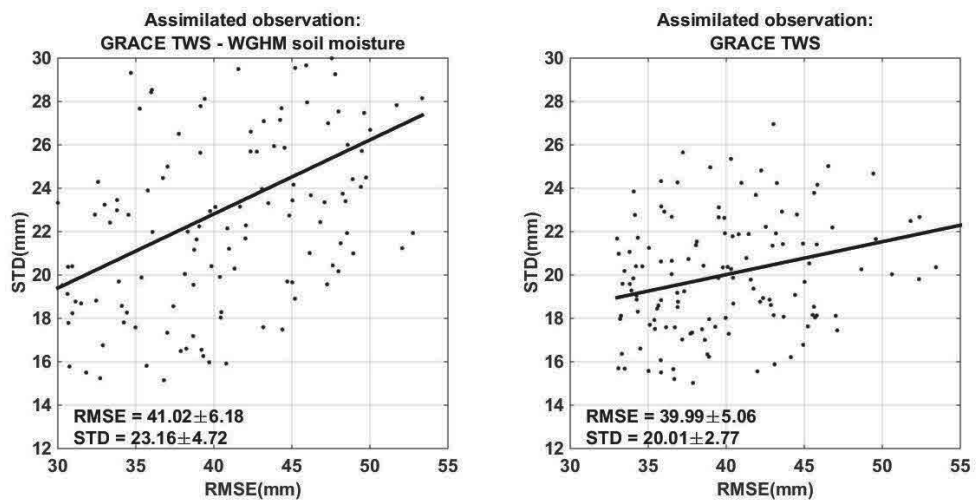


Figure 6: Average groundwater RMSE and STD from assimilating GRACE TWS and GRACE TWS minus soil moisture.

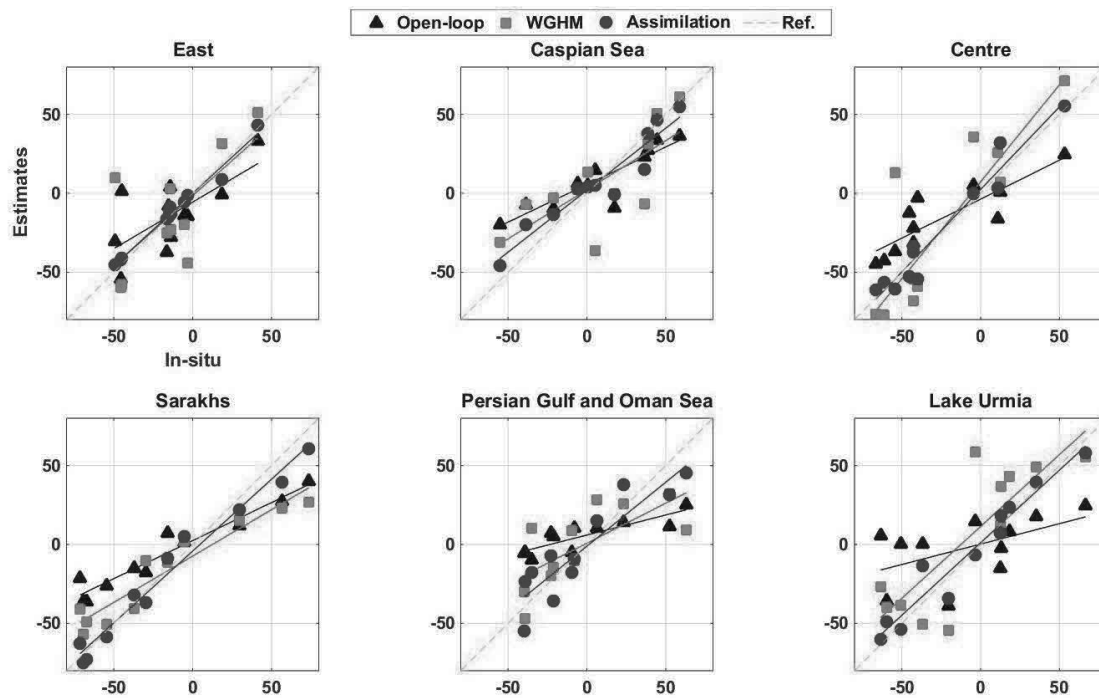


Figure 7: Comparison between in-situ groundwater measurements and those estimated by open-loop run, data assimilation, and WGHM over different catchments (units are mm).

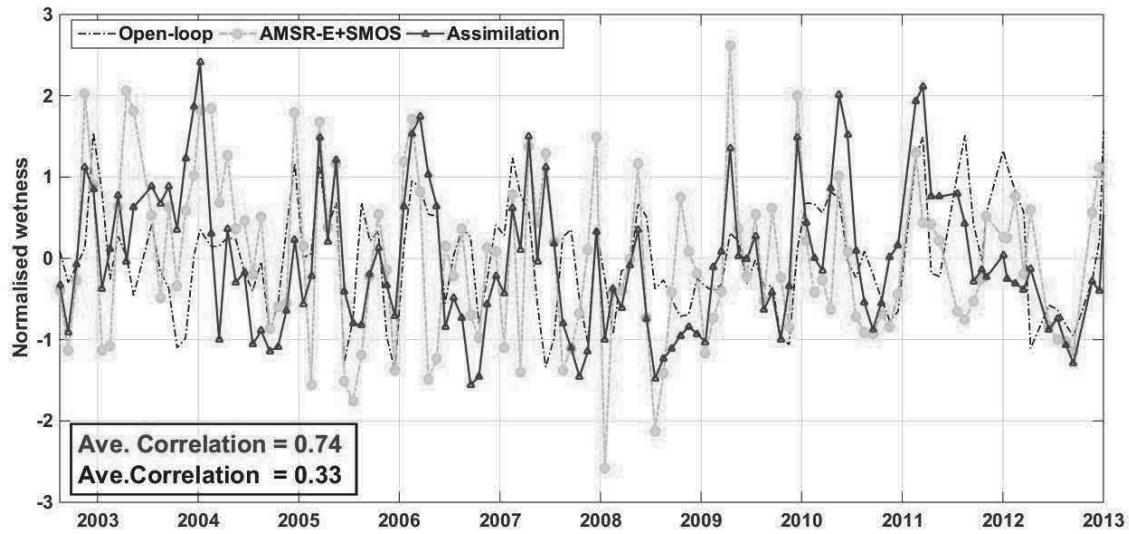


Figure 8: Comparison between the average estimated top layer soil moisture with and without (open-loop) data assimilation and soil moisture observations from satellite remote sensing (AMSR-E+SMOS). Correlations between the satellite measurements and both open-loop and assimilation estimates are also reported in the figure.

2353
2354
2355
2356
2357
2358
2359
2360
2361
2362
2363
2364
2365
2366
2367
2368
2369
2370
2371
2372
2373
2374
2375
2376
2377
2378
2379
2380
2381
2382
2383
2384
2385
2386
2387
2388
2389
2390
2391
2392
2393
2394
2395
2396
2397
2398
2399
2400
2401
2402
2403
2404
2405
2406
2407
2408

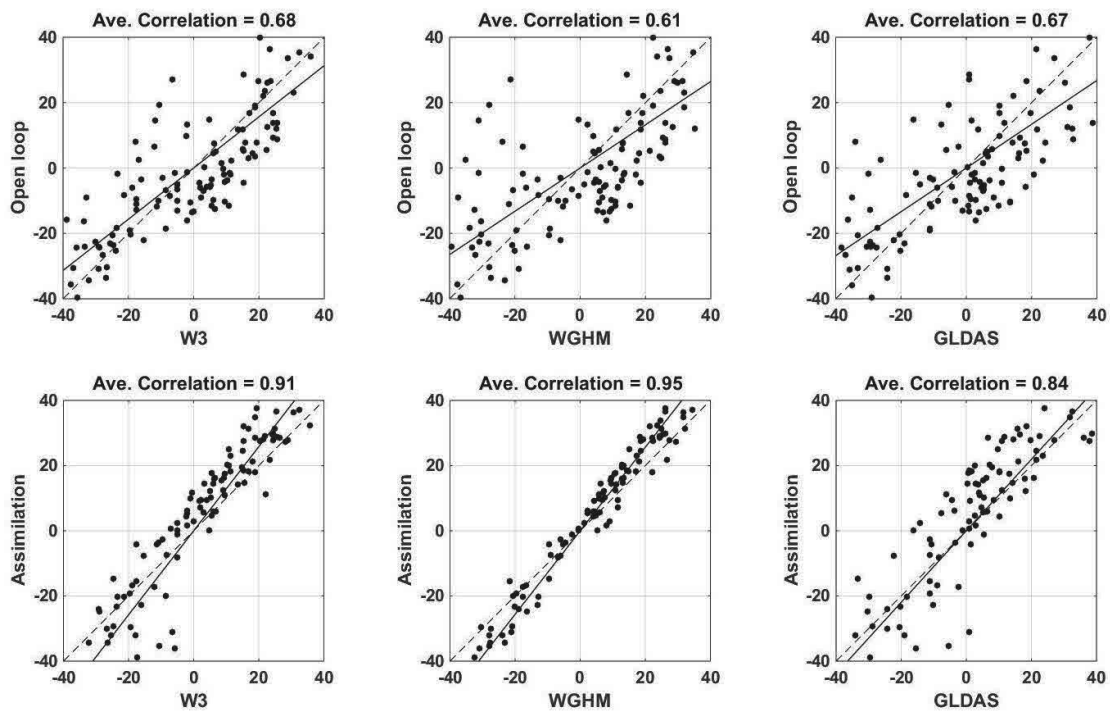


Figure 9: Comparison between the average soil moisture estimates from open-loop and data assimilation, and soil moisture products of W3, WGHM, and GLDAS (units are mm).

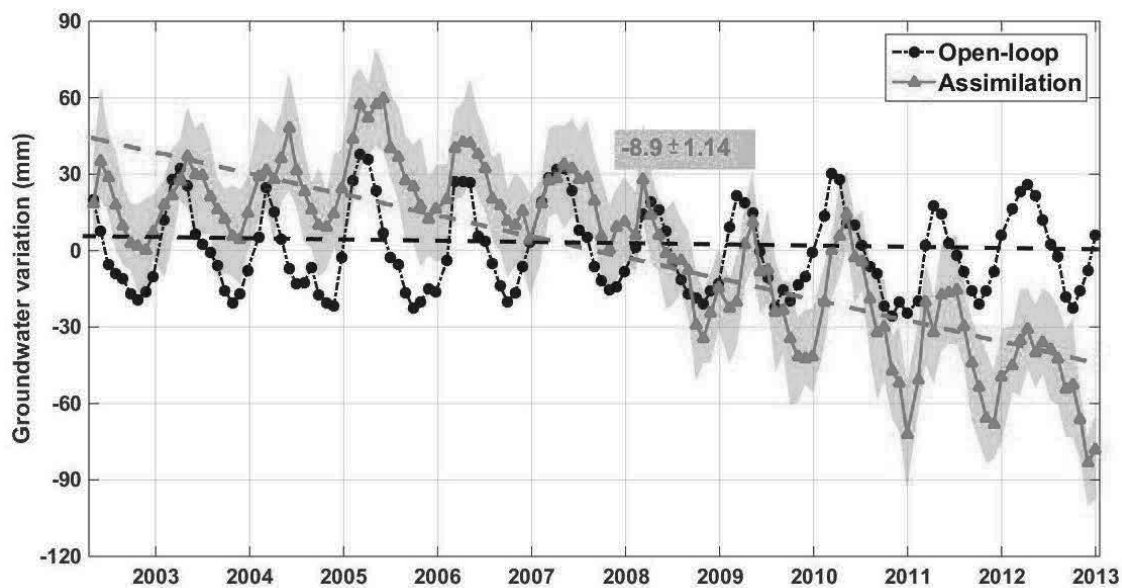


Figure 10: Average groundwater variations within Iran from open-loop and data assimilation results and corresponding 95% confidence intervals (shaded blue). Trend lines for time series are also displayed by dashed lines. Note that the open-loop time series slope is not reported because no significant trend is observed.

2465
2466
2467
2468
2469
2470
2471
2472
2473
2474
2475
2476
2477
2478
2479
2480
2481
2482
2483
2484
2485
2486
2487
2488
2489
2490
2491
2492
2493
2494
2495
2496
2497
2498
2499
2500
2501
2502
2503
2504
2505
2506
2507
2508
2509
2510
2511
2512
2513
2514
2515
2516
2517
2518
2519
2520

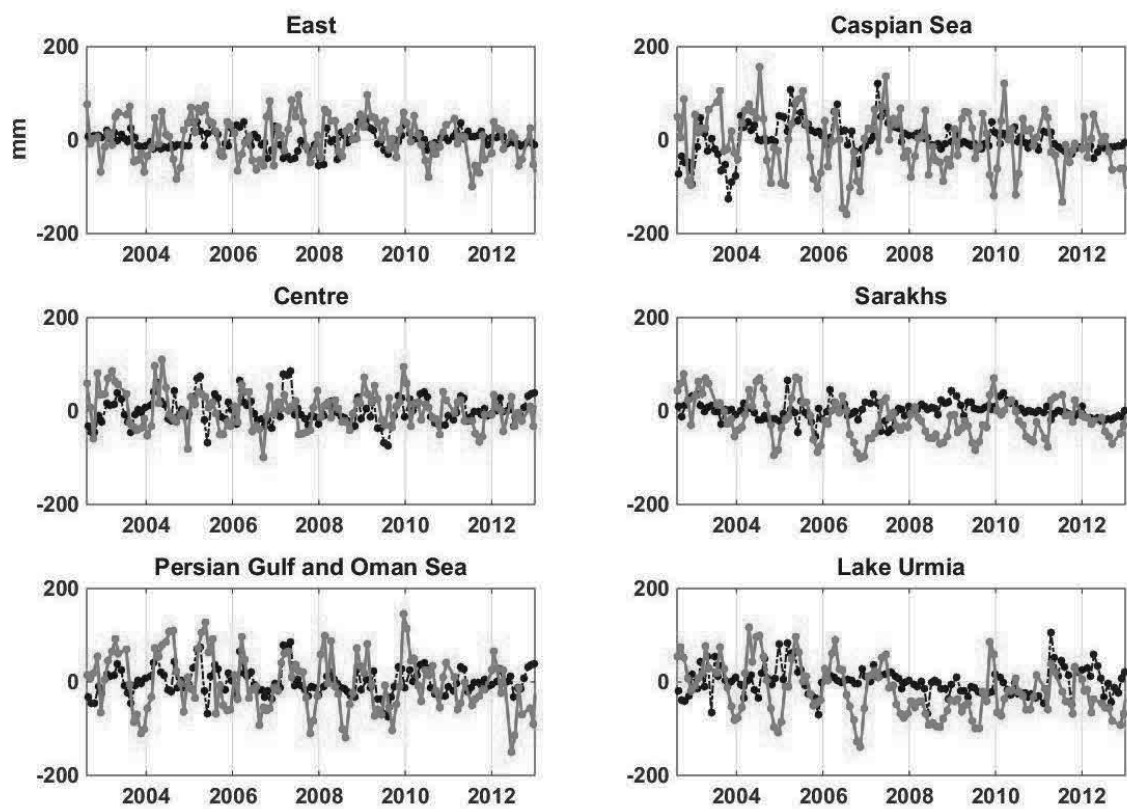


Figure 11: Average time series of soil moisture variations over different catchments with (blue) and without (black) data assimilation.

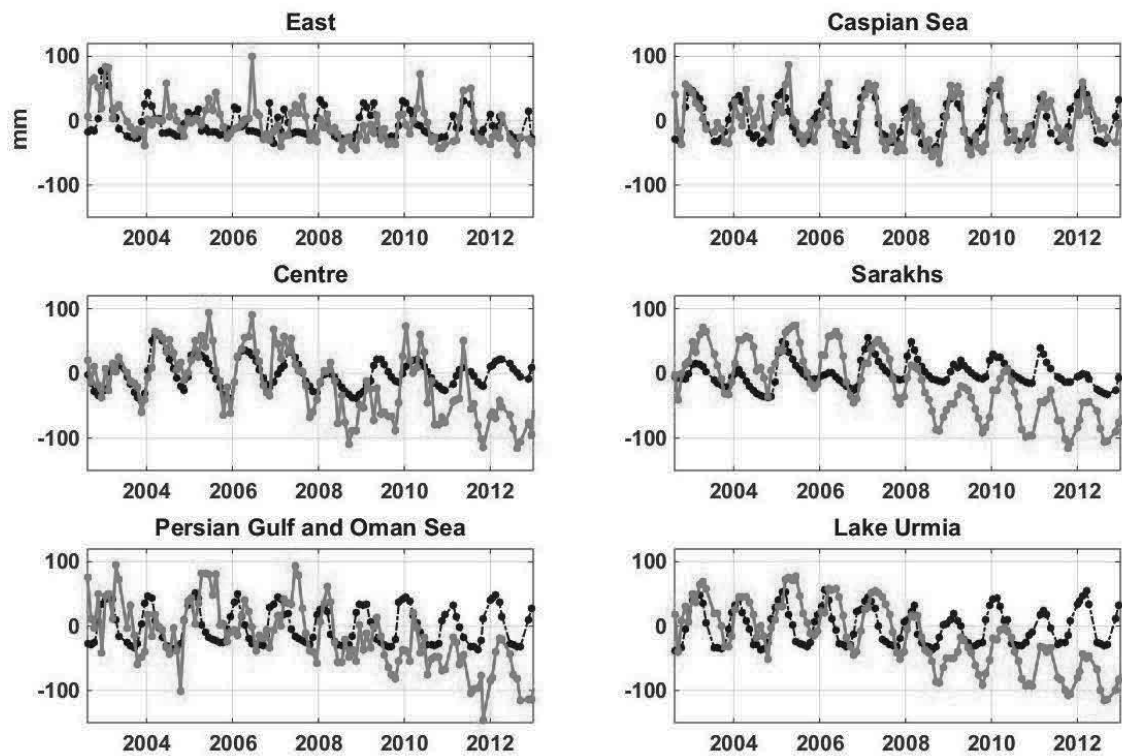


Figure 12: Average time series of groundwater variations over different catchments with (blue) and without (black) data assimilation. The correlations of time series with the in-situ measurements, as well as the trends of assimilation results are reported in Table 2.

2577
2578
2579
2580
2581
2582
2583
2584
2585
2586
2587
2588
2589
2590
2591
2592
2593
2594
2595
2596
2597
2598
2599
2600
2601
2602
2603
2604
2605
2606
2607
2608
2609
2610
2611
2612
2613
2614
2615
2616
2617
2618
2619
2620
2621
2622
2623
2624
2625
2626
2627
2628
2629
2630
2631
2632

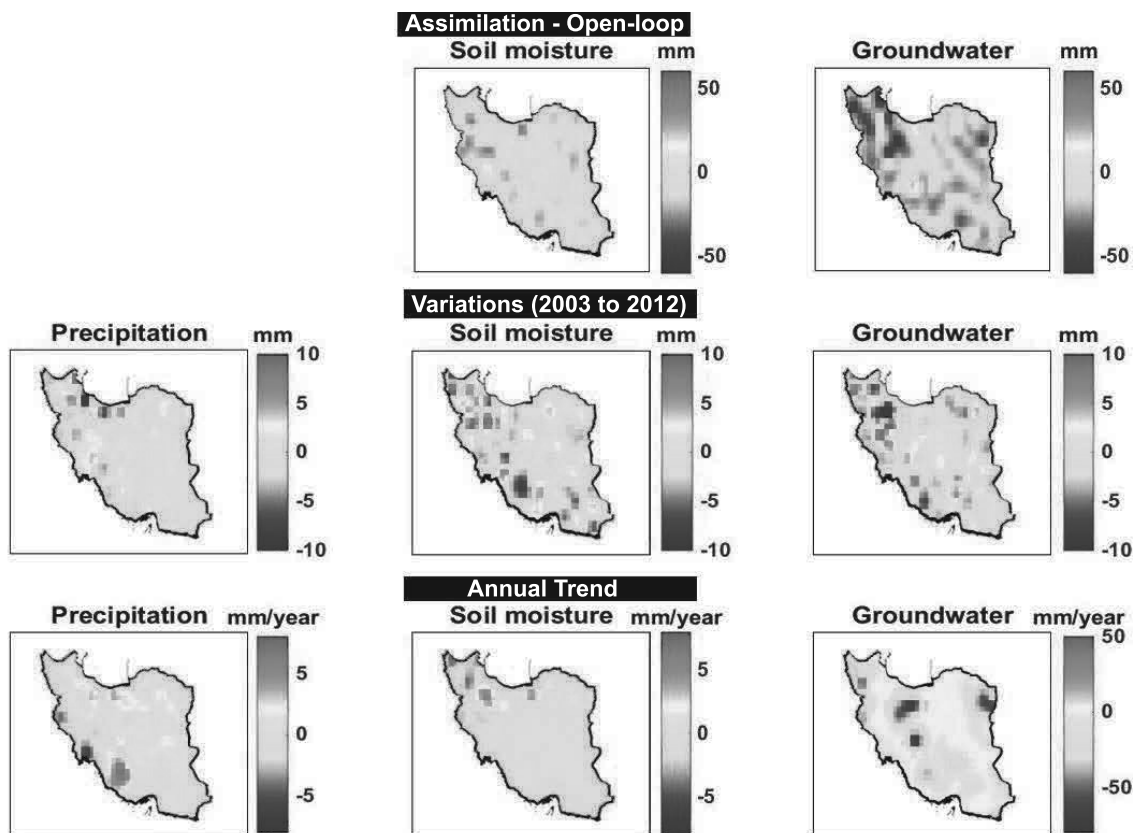


Figure 13: First row: temporally averaged increments applied to soil moisture and groundwater storages. Second row: variation of precipitation, soil moisture, and groundwater (after data assimilation) estimated as the average of each time series at each grid point. Third row: gridded trend of time series precipitation, soil moisture, and groundwater (after data assimilation) time series.

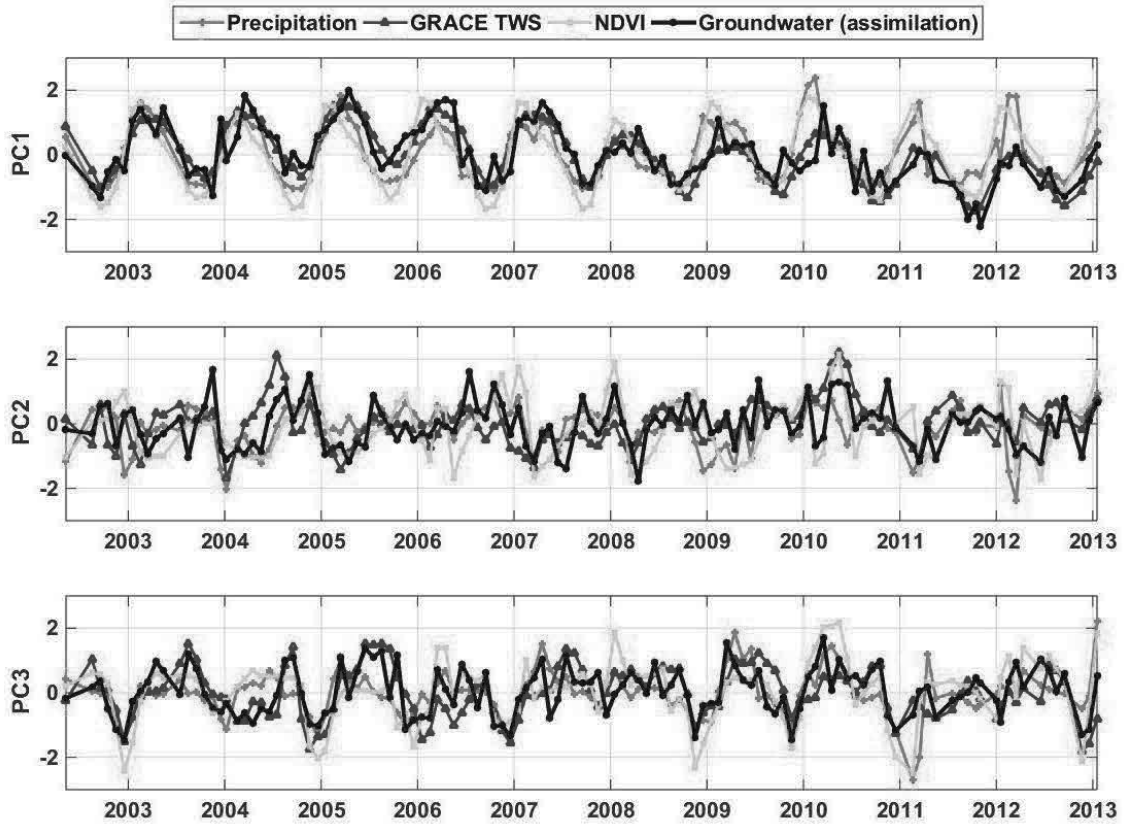


Figure 14: The three first principal components of precipitation, GRACE TWS, NDVI, and groundwater.

2689
2690
2691
2692
2693
2694
2695
2696
2697
2698
2699
2700
2701
2702
2703
2704
2705
2706
2707
2708
2709
2710
2711
2712
2713
2714
2715
2716
2717
2718
2719
2720
2721
2722
2723
2724
2725
2726
2727
2728
2729
2730
2731
2732
2733
2734
2735
2736
2737
2738
2739
2740
2741
2742
2743
2744

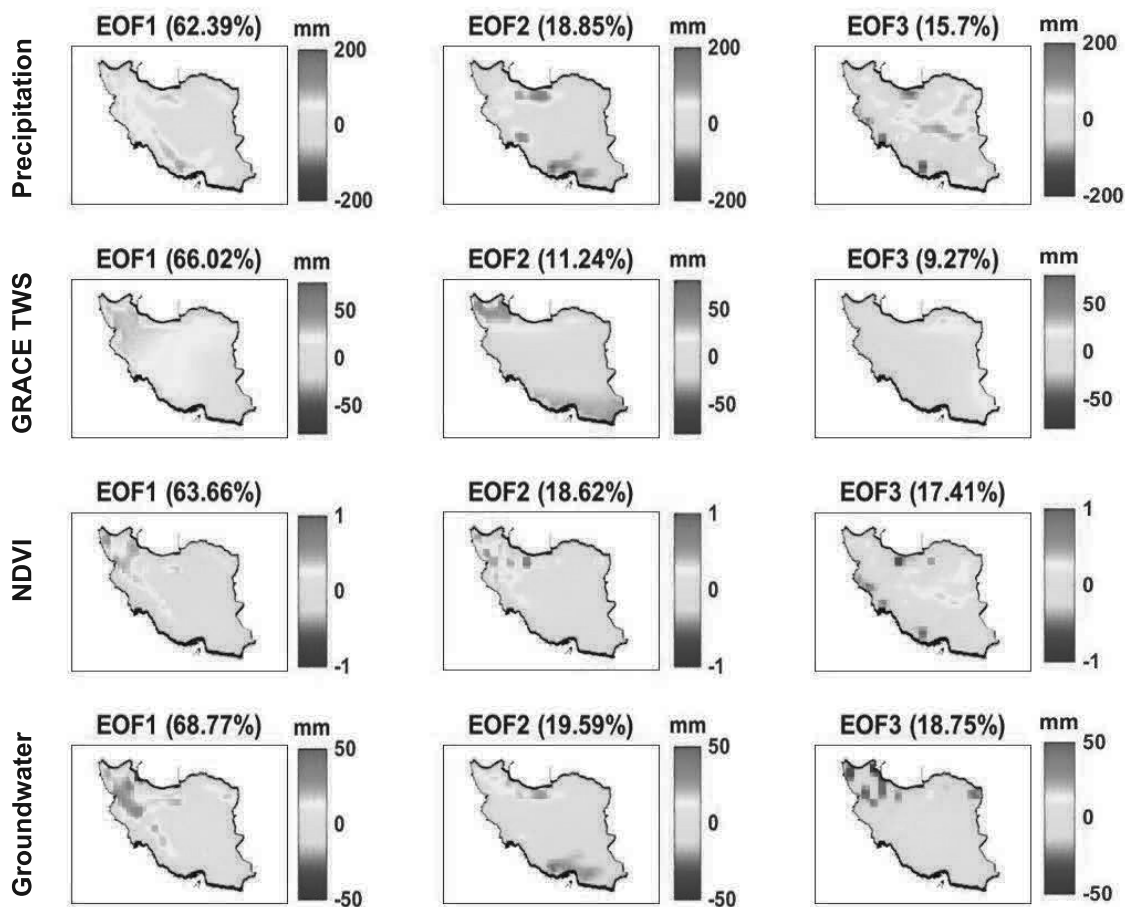


Figure 15: The empirical orthogonal functions (EOF1, EOF2, and EOF3) extracted from precipitation, GRACE TWS, NDVI, and groundwater.

2745
2746
2747
2748
2749
2750
2751
2752
2753
2754
2755
2756
2757
2758
2759
2760
2761
2762
2763
2764
2765
2766
2767
2768
2769
2770
2771
2772
2773
2774
2775
2776
2777
2778
2779
2780
2781
2782
2783
2784
2785
2786
2787
2788
2789
2790
2791
2792
2793
2794
2795
2796
2797
2798
2799
2800

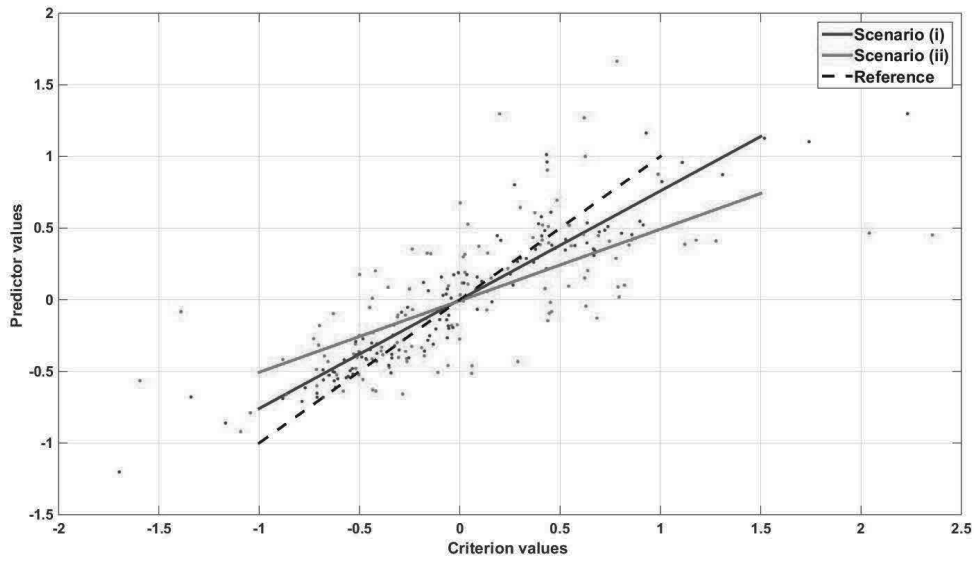


Figure 16: Scatter bi-plots (circles) and the linear trend (solid lines) of average canonical coefficients from CCA for each scenario applied. The combination of the water storages and discharge data and their canonical coefficients are in the x-axis (as criterion variables), the y-axis represents the combination of the predictor variables. Black solid line represents the reference line.

2801
 2802
 2803
 2804
 2805
 2806
 2807
 2808
 2809
 2810
 2811
 2812
 2813
 2814
 2815
 2816
 2817
 2818
 2819
 2820
 2821
 2822
 2823
 2824
 2825
 2826
 2827
 2828
 2829
 2830
 2831
 2832
 2833
 2834
 2835
 2836
 2837
 2838
 2839
 2840
 2841
 2842
 2843
 2844
 2845
 2846
 2847
 2848
 2849
 2850
 2851
 2852
 2853
 2854
 2855
 2856

Table 1: A summary of the datasets used in this study.

Description	Platform	Data access
Terrestrial water storage (TWS)	GRACE	https://www.tugraz.at/institute/ifg/downloads/gravity-field-models/itsg-grace2014/
Precipitation	TRMM-3B43	https://disc.gsfc.nasa.gov/datacollection/TRMM_3B43_7.html
Normalized Difference Vegetation Index (NDVI)	NASA-GSFC	ftp://eclipse.ncdc.noaa.gov/pub/cdr/avhrr-land/ndvi/
Hydrological model	W3RA	http://www.wenfo.org/wald/data-software/
Temperature	Harris (2008)	https://crudata.uea.ac.uk/cru/data/hrg/
Groundwater in-situ measurements	IWRMC	http://www.wrm.ir/
Average water consumption	IWRMC	http://www.wrm.ir/
Discharge data	IWRMC	http://www.wrm.ir/
Number of groundwater bore holes	IWRMC	http://www.wrm.ir/
Altimetry-derived level height	Jason-1	http://podaac.jpl.nasa.gov
Altimetry-derived level height	Jason-2	http://avisoftp.cnes.fr/

2857
2858
2859
2860
2861
2862
2863
2864
2865
2866
2867
2868
2869
2870
2871
2872
2873
2874
2875
2876
2877
2878
2879
2880
2881
2882
2883
2884
2885
2886
2887
2888
2889
2890
2891
2892
2893
2894
2895
2896
2897
2898
2899
2900
2901
2902
2903
2904
2905
2906
2907
2908
2909
2910
2911
2912

Table 2: The undertaken experiments and corresponding research objectives. The result section associated to each experiment is also presented.

Experiment	Research objective	Result section
Simulated assimilation	To assess the impacts of GRACE observations on different water storage	Section 4.1
Evaluation procedure	To examine the validity of results against independent observations	Section 4.2
Water storage analysis	To analyze spatio-temporal variations of groundwater and soil moisture	Section 4.3
Climatic impacts using PCA	To investigate the impacts of climate indicators (e.g., precipitation) on water storage	Section 4.4
CCA	To establish the relations between water storages and human- as well as climate-related variables	Section 4.5

Table 3: Statistics of groundwater variations and its errors with respect to the in-situ observations. For each region the RMSE average and its range ($\pm XX$) at the 95% confidence interval is presented. Improvements in data assimilation results are calculated for each catchment in relation to the water storages from the model without implementing data assimilation.

Region	Groundwater trend (mm/year)	Assessment with In-situ				Improvement (%)
		Open-loop		Assimilation		
		Correlation	RMSE (mm)	Correlation	RMSE (mm)	
East	-3.8	0.57	60±8.66	0.84	38±4.64	36.29
Caspian Sea	-2.1	0.64	64±9.19	0.73	46±5.13	28.13
Centre	-6.7	0.63	55±7.84	0.65	41±5.01	26.55
Sarakhs	-5.4	0.61	52±7.58	0.82	32±4.26	38.64
Persian Gulf and Oman Sea	-9.3	0.56	79±9.07	0.75	49±5.17	37.81
Lake Urmia	-11.8	0.52	69±8.28	0.81	40±4.25	41.90

Table 4: Average canonical correlation coefficients and variable loadings for the data inputs in CCA for each scenario.

		Scenario (i)	Scenario (ii)
		Canonical coefficients	Canonical coefficients
Canonical correlation coefficient		0.972	0.841
Predictor variables	Precipitation	0.721	0.749
	NDVI	0.365	0.412
	Temperature	-0.591	-0.681
	Water use for: # Farming	-0.938	-
	# Industry	-0.758	-
	# Drink (Urban use)	-0.820	-
	Number of bore holes	-0.893	-
Criterion variables	Groundwater	0.938	0.705
	Soil moisture	0.633	0.617
	Water discharge	0.174	0.249